UNIVERSITY OF THESSALY

SCHOOL OF ENGINEERING

DEPARTMENT OF MECHANICAL ENGINEERING

ALTERNATIVE ENERGY CONVERSION SYSTEMS LABORATORY

ΠΑΝΕΠΙΣΤΗΜΙΟ
ΘΕΣΣΑΛΙΑΣ

Thesis

PRODUCTION AND CHARACTERIZATION OF EFFICIENT LOW-COST ELECTRODES FOR FUEL CELLS (H_2-PEMFC)

by

NIKOLAOS MALAMAS

STAVROS KATSAROS

Submitted in fulfillment of the requirements for the Diploma in the Department of Mechanical Engineering of the University of Thessaly

Volos 2017

Η έγκριση της διπλωματικής εργασίας από το Τμήμα Μηχανολόγων Μηχανικών Βιομηχανίας της Πολυτεχνικής Σχολής του Πανεπιστημίου Θεσσαλίας δεν υποδηλώνει αποδοχή των απόψεων του συγγραφέα (Ν. 5343/32 αρ. 202 παρ. 2).

Εγκρίθηκε από τα Μέλη της Τριμελούς Εξεταστικής Επιτροπής:

Examiner: Dr Panagiotis Tsiakaras
(Supervisor) Professor, Department of Mechanical Engineering,
University of Thessaly

Examiner: Dr Stapountzis Herricos
Professor, Department of Mechanical Engineering,
University of Thessaly

Examiner: Dr Brouzgou Angeliki
Senior Researcher & Teaching Staff,
Department of Mechanical Engineering,
University of Thessaly

Acknowledgements

The following thesis was carried out in the Alternative Energy Conversion Systems Laboratory of the Department of Mechanical Engineering of the University of Thessaly. Reached the end of this long and hard journey, we would like to express our gratitude to our thesis supervisor, Professor Tsiakaras Panagiotis for his vision in proposing such an interesting thesis theme. During the present study we made many challenging discussions, with many ups and down moments, leading to a fruitful strategic conduction of the thesis. In all aspects, we are grateful and we feel the necessity to express our gratitude to him. We would also like to thank for their time and their useful advices the members of the examination committee: Prof. Stapountzis Herricos and Dr Brouzgou Angeliki.

We are also thankful to Alternative Conversion Systems Laboratory's Research Group for their support and help regarding the completion of our dissertation. More precisely, we would like firstly to thank, Dr Sotiria Kontou for her support and encouragement. We would like to thank our colleagues and good friends Antonis Vouzavalis and Stergios Georgantas for their interesting and rewarding suggestions. Finally, during the thesis, we received invaluable help from Dr Brouzgou Angeliki, who we are indebted we had the pleasure to work with.

During our thesis study, life would be much more difficult without the support and companionship of our best friends. Finally, we owe the deepest gratitude to our beloved families, for their support and continuous encouragement during our studies.

Malamas Nikolaos

Katsaros Stavros

Abstract

In today's world, the demand for clean and sustainable energy sources has become a strong driving force in a constant economic development. Although energy levels remain stable, human's inability highly-efficient conversion of energy (~30%) leads to environmental degradation. Researchers focus on two main solutions, 1) optimization of conventional internal combustion engines and 2) construction of new more efficient devices. Proton exchange membranes (PEM) fuel cells as clean energy converting devices have drawn a great deal of attention in recent years due to their high efficiency, high energy density and low or zero emissions. However, the major barriers to the widespread use and commercialization of fuel cells are, firstly, the rate determining step of the procedure. The ORR reaction is almost 10 times slower than the HOR. Secondly, their high cost (mainly due to the extensively adopted Platinum-based nano-materials, used as catalysts) and low reliability/durability. Thus, the limited resources of Platinum increased the interest of the scientific community towards the exploration of Pt-free electrocatalysts. In the present work Vulcan XC-72 carbon supported Pd, Ir and Pd_xIr_y (with x:y atomic ratios 3:1, 1:1, 1:3) electrocatalysts catalysts are thoroughly investigated for the reactions of Hydrogen oxidation and Oxygen reduction (HOR and ORR). Catalysts are prepared via a pulse-microwave assisted polyol method. The techniques of X-ray diffraction (XRD) and Transmission Electron Microscopy (TEM) permitted to investigate the elemental composition, the structure, and the morphology of the catalysts. Their electrocatalytic properties toward the reactions of Hydrogen Oxidation and Oxygen Reduction are evaluated by the aid of cyclic voltammetry (CV) and rotating disk electrode (RDE) techniques. It is found that the electrocatalytic activity of pure Pd is enhanced, toward both HOR and ORR, after the addition of an even small amount of Ir. According to the results the highest HOR and ORR electrocatalytic activity enhancement is exhibited by PdIr. The order of electrocatalytic activity over the as prepared electrode materialsis found to be PdIr>$PdIr_3$>Pd_3Ir>Pd>Ir for HOR and PdIr> Pd_3Ir > $PdIr_3$>Pd>Ir for the ORR.

Περίληψη

Στην σημερινή εποχή, η ζήτηση για καθαρές και βιώσιμες πηγές ενέργειας έχει καταστεί ισχυρή κινητήρια δύναμη για μια συνεχή οικονομική ανάπτυξη. Παρόλο που τα αποθέματα ενέργειας του πλανήτη παραμένουν σταθερά, η δυσκολία του ανθρώπου να τα χρησιμοποιήσει και να τα μετατρέψει αποδοτικά (~30%) οδηγεί στην υποβάθμισή τους. Οι ερευνητές στοχεύουν σε δύο βασικές λύσεις, 1) Βελτιστοποίηση των συμβατικών μηχανών μετατροπής ενέργειας, 2) Κατασκευή νέων πιο αποδοτικών μηχανών. Οι μεμβράνες ανταλλαγής πρωτονίων (PEM) ως συσκευές μετατροπής καθαρής ενέργειας έχουν προσελκύσει μεγάλο ενδιαφέρον τα τελευταία χρόνια λόγω της υψηλής απόδοσης, της υψηλής ενεργειακής πυκνότητας και των χαμηλών ή μηδενικών εκπομπών τους. Ωστόσο, το κύριο εμπόδιο για την ευρεία χρήση και εμπορευματοποίηση των κυψελών καυσίμου είναι, αρχικά, το βραδύ βήμα της εξίσωσης. Η αναγωγή του οξυγόνου είναι 10 φορές πιο αργή από την οξείδωση του υδρογόνου. Καθώς και το υψηλό κόστος τους (κυρίως λόγω των νανοϋλικών που χρησιμοποιούνται ως καταλύτες με βάση την πλατίνα) και της χαμηλής αξιοπιστίας / ανθεκτικότητας. Έτσι, οι περιορισμένοι πόροι της πλατίνας αύξησαν το ενδιαφέρον της επιστημονικής κοινότητας για την διερεύνηση ηλεκτροκαταλυτών χωρίς Pt. Στην παρούσα εργασία οι καταλύτες Pd, Ir και Pd_xIr_y (με αναλογίες x:y ατομικών αναλογιών 3: 1, 1: 1, 1: 3) σε άνθρακα Vulcan XC-72 διερευνώνται διεξοδικά για τις αντιδράσεις της οξείδωσης του υδρογόνου και της αναγωγής οξυγόνου (HOR και ORR). Οι καταλύτες παρασκευάζονται μέσω υποβοηθούμενης μεθόδου πολυόλης με τη βοήθεια παλμού-μικροκυμάτων. Οι τεχνικές της περίθλασης ακτίνων X (XRD) και της ηλεκτρονικής μικροσκοπίας μετάδοσης (TEM) επέτρεψαν τη διερεύνηση της στοιχειακής σύνθεσης, της δομής και της μορφολογίας των καταλυτών. Οι ηλεκτροκαταλυτικές ιδιότητές τους ως προς τις αντιδράσεις της οξείδωσης του υδρογόνου και της αναγωγής οξυγόνου αξιολογούνται με τη βοήθεια τεχνικών κυκλικής βολταμετρίας (CV) και ηλεκτροδίων περιστρεφόμενου δίσκου (RDE). Αποδείχτηκε ότι η ηλεκτροκαταλυτική δραστικότητα του καθαρού Pd είναι ενισχυμένη, τόσο προς την HOR όσο και προς την ORR, μετά την προσθήκη μίας ακόμη μικρής ποσότητας Ir. Σύμφωνα με τα αποτελέσματα, η υψηλότερη ενίσχυση της ηλεκτροκαταλυτικής δραστηριότητας HOR και ORR εκδηλώνεται από το PdIr. Η σειρά της ηλεκτροκαταλυτικής δραστικότητας έναντι των υλικών ηλεκτροδίων που παρασκευάστηκαν με τον τρόπο αυτό είναι PdIr>$PdIr_3$>Pd_3Ir>Pd>Ir για HOR και PdIr>Pd_3Ir>$PdIr_3$>Pd>Ir για το ORR.

CONTENTS

LIST OF FIGURES

LIST OF TABLES

CHAPTER I

1 INTRODUCTION

Abstract

In the present chapter, global energy crisis is being taken under consideration as well as the continuous development of renewable energy sources' technology. Moreover, electrochemistry fundamentals are presented aiming to assist the viewer's better understanding of the electrochemical devices.

1.1 Energy Crisis- Environmental Threats- Alternative Solutions

Environmental degradation, population growth and resource consumption are several vital challenges the world faces nowadays. The perils of global warming such as global warming, climate change and energy crisis are continuously threatening the environment. Global warming occurs when gases like carbon dioxide and methane stay trapped in the earth's atmosphere. This carbon overload is caused mainly by burning fossil fuels like coal, oil/petrol and natural gas or cutting down and burning forests. There are many heat-trapping gases (from methane to water vapor), but CO_2 exposes us at the greatest risk of irreversible changes if it continues to accumulate unabated in the atmosphere[1].These gases are known as "greenhouse gases" due to their capacity to retain heat. In general, this phenomenon is well-known as the "greenhouse effect"[2]. This effect leads to an increase in global temperature which in turn is the cause of global climate change. Land degradation, air and water pollution, sea-level rise, flood of coastal areas and loss of biodiversity are only several consequences of climate change.

Resolving the problem of climate change requires multiple, long-term strategies which demand enormous accumulated efforts, engaging the cooperation of

both developed and developing countries. Currently, developed countries are responsible for the larger share of greenhouse gas emissions, but developing countries' emissions continue to rise steadily. It is estimated that by the year 2025, emissions of developing countries are expected to represent 50% of the global total. This calls for immediate and globally coordinated actions[1].

The demand of energy is growing day by day due to increasing industrialization and population. Self-sufficiency in energy is the assurance to excel any country's economy and vital for sustainable development. According to International Energy Agency (IEA) world energy outlook 2005, energy demand will increase by 50% by 2030[3].Methods of production, supply and consumption of energy are key issues in sustainable development because they strongly affect the local and global environment. However, the current means of energy production are primarily originated from the use of fossil fuels.

Fossil energy sources used to solve every energy problem such as a variety of domestic, transport and industrial needs. However, fossil fuels cannot continue indefinitely as the principal energy sources due to the rapid increase of world energy demand and energy consumption. They are non-renewable sources of energy as they derive from pre-historic fossils and will not be available once they are fully used. Their sources are limited and they are depleting at a fast rate. As a consequence, investigations of alternative energy strategies have recently become important particularly for future world stability[1]. From this aspect, renewable sources such as hydroelectric power[4, 5], biomass[6], solar[7], wind[7] and geothermal energy[8] are being investigated in order to produce mainly electricity, but bio-fuels[9-11] (bio-diesel[12], bio-ethanol[13] or bio-methanol[14]) are also under the microscope. Furthermore, the most important asset of alternative energy sources is the environmental compatibility. From this perspective, hydrogen is likely to become one of the most attractive energy carriers in the near future[15].

In recent years, researchers' efforts are focused on the optimization and expansion of electrochemical devices which provide safe, environmentally friendly and reliable energy supplies[16]. Fuel cells, which are a distinctive example of the electrochemical devices, are considered to be a viable clean-air alternative not only for applications of internal combustion engine, but also for many conventional power supply technologies. They are capable of efficient replacement of current battery

technology and meet the future demand for portable electric power supplies. In addition, fuel cells can operate on hydrogen or a variety of gaseous and liquid hydrocarbons fuels, which are less harmful than the conventional fuels. In the following parts of this study, electrochemical devices and especially fuel cells will be investigated thoroughly[17].

1.2 Electrochemistry basics concerning electrochemical devices

At this point, it is vital to mention that all electrochemical devices have a great correlation with the fundamentals of electrochemistry. In general, electrochemistry deals with the interaction between electrical energy and chemical change[18].More specifically, electrochemistry is the study of chemical processes that cause electrons to move. This movement of electrons is called electricity, which can be generated by the transfer of electrons from one element to another in a reaction known as an oxidation-reduction ("redox") reaction[19].

A redox reaction is a reaction that describes the change of oxidation state that take place in the atoms, ions or molecules involved in an electrochemical reaction. When a substance (atom, ion or molecule) loses an electron, its oxidation state increases and the whole process is called oxidation. On the other hand, when a substance gains an electron, its oxidation state decreases and, respectively, the process is referred as reduction. Hence, the overall reaction can be described as two-half reactions, as it is impossible to have a reduction without oxidation and vice versa. In addition, the substance which loses electrons is called the reducing agent or reductant, whereas the substance which accepts the electrons is known as the oxidizing agent or oxidant. Thus, the oxidant is always being reduced in a reaction, whereas the reductant is always being oxidized[18, 19]. For example, for the reaction of zinc (Zn) with bromine (Br_2), the overall chemical reaction is:

$$Zn_{(s)} + Br_{2(aq)} \rightarrow Zn^{2+}_{(aq)} + 2Br^{-}_{(aq)} \quad (1)$$

And it can be written as:

- Oxidation reaction

$$Zn_{(s)} \rightarrow Zn^{2+}_{(aq)} + 2e^{-} \quad (1.1)$$

- Reduction reaction

$$Br_{2(aq)} + 2e^{-} \rightarrow 2Br^{-}_{(aq)} \quad (1.2)$$

Thus, the aforesaid reactions show that Zn is the reductant and Br_2 is the oxidant in the overall redox reaction (equation 1), which is proven by adding equations 1.1 and 1.2. Additionally, a redox reaction is balanced when the number of electrons lost by the reductant equals the number of electrons gained by the oxidant. Like any balanced chemical equation, the overall process is electrically neutral; that is because the net charge is the same on both sides of the equation[20].

In most chemical reactions, the reactants are in intimate physical contact with one another. For example, acid–base reactions are usually carried out with the acid and the base dispersed in a single phase, such as a liquid solution. In redox reactions, however, it is possible to separate physically the oxidation and reduction half-reactions in space. A complete circuit, including an external electrical connection, such as a wire between the two-half reactions, is responsible for that separation. As the reaction progresses, the electrons flow from the reductant to the oxidant over this electrical connection, producing an electric current that can be used to do work, for example to turn a motor or power a light. An apparatus that is used to generate electricity from a spontaneous redox reaction or, conversely, that uses electricity to drive a non-spontaneous redox reaction is called an electrochemical cell[20].

There are two types of electrochemical cells: voltaic or galvanic cells and electrolytic cells. In the late 18th century, the Italian physician and anatomist Luigi Galvani (1737-1798), observed that dissected frog leg muscles twitched when a small electric shock was applied. That was enough information in order to force him to demonstrate the electrical nature of nerve impulses[21]. At the same period, in 1793, the Italian physicist and chemist Alessandro Volta (1745-1827), discovered that electricity could be produced by placing different metals on the opposite sides of a

wet paper or cloth. He made his first battery by placing Ag and Zn on the opposite sides of a moistened cloth with salt or weak acid solution. Therefore, a galvanic (voltaic) cell is an electrochemical cell which uses the energy released during a spontaneous redox reaction ($\Delta G < 0$) in order to generate electricity. In contrast, an electrolytic cell consumes electrical energy from an external source, using it to cause a non-spontaneous redox reaction to occur ($\Delta G > 0$)*(Figure 1)*[20].

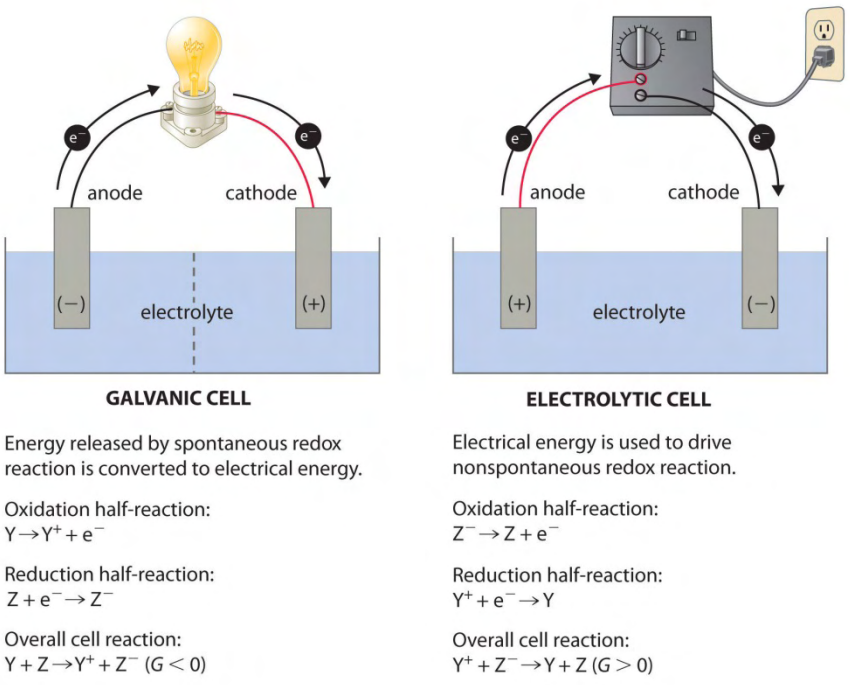

Figure 1.1. A typical depiction of a galvanic (voltaic) and an electrolytic cell [20]

A galvanic (voltaic) cell, as well as an electrolytic cell which follows a similar operating principle, consists of two compartments called half-cells. Each half-cell includes an electrode and an electrolyte. Electrodes can be made from any sufficiently conductive materials, such as metals, semi-conductors, graphite and even conductive polymers. Basically, the electrode can be made from an inert, highly conductive metal such as platinum to prevent it from reacting during a redox process; meanwhile, it (Pt) does not appear in the overall electrochemical reaction. In addition, each half-cell may use the same or different electrolyte, which is an ionic substance or solution that allows ions to transfer between the electrode compartments, maintaining the system's electrical neutrality. The oxidation half-reaction occurs at one electrode which is called anode, whereas the reduction half-reaction occurs at the other, which is called cathode. The two electrodes must be electrically connected (closed circuit) to each

other, allowing the flow of electrons from the negative electrode (anode) to the positive electrode (cathode).As the negatively charged electrons flow in one direction through the circuit, the positively charged metal ions flow in the opposite direction in the electrolyte[18, 20].

A salt bridge, which consists of an electrolyte saturated gel (filter paper soaked in KNO_3, NaCl, etc.) in an inverted U-shaped tube, is also required to maintain electrical neutrality and allow the reaction to proceed. Moreover, it is used in order to provide ionic contact between the anode and the cathode electrolytes, and prevent the solutions from mixing and causing unwanted side reactions. Thus, salt bridge is a porous plug that allows ion flow while reducing electrolyte mixing. In the absence of a salt bridge or some other similar connection, the reaction would rapidly cease because electrical neutrality could not be maintained[18, 20].

In conclusion, a distinct example of galvanic cell is the so-called Daniell cell, in honor of John Frederic Daniell (1790-1845), who invented this pioneering device in 1836. More specifically, this electrochemical setup (not the original one, but a practical evolution of it) could be seen in *Figure 2* and described as it follows: a copper strip is inserted into a beaker that contains a 1 M solution of Cu^{2+} ions as a zinc strip is inserted into a different beaker that contains a 1 M solution of Zn^{2+} ions. Generally, when a zinc rod is inserted into a beaker that contains an aqueous solution of copper (II) sulfate, a spontaneous redox reaction occurs: the zinc electrode dissolves to give Zn^{2+}(aq) ions, while Cu^{2+}(aq) ions are simultaneously reduced to metallic copper. The reaction occurs so rapidly that the copper is deposited as very fine particles that appear black, rather than the usual reddish color of copper. Then, the two metal strips, which play the role of electrodes, are connected by a wire, as the two compartments are joined up with a salt bridge. The ions in the salt bridge are selected so that they do not interfere with the electrochemical reaction. From this perspective, there is a risk of being oxidized or reduced as well as forming a precipitate or complex. So, most commonly used cations and anions are Na^+ or K^+ and NO_3^- or SO_4^{2-}, respectively. When the circuit is closed, a spontaneous reaction occurs: zinc metal is oxidized to Zn^{2+} ions at the zinc electrode (the anode), and Cu^{2+} ions are reduced to Cu metal at the copper electrode (the cathode). As the reaction progresses, the zinc strip dissolves, and the concentration of Zn^{2+} ions in the Zn^{2+}

solution increases; simultaneously, the copper strip gains mass, and the concentration of Cu^{2+} ions in the Cu^{2+} solution decreases[20].

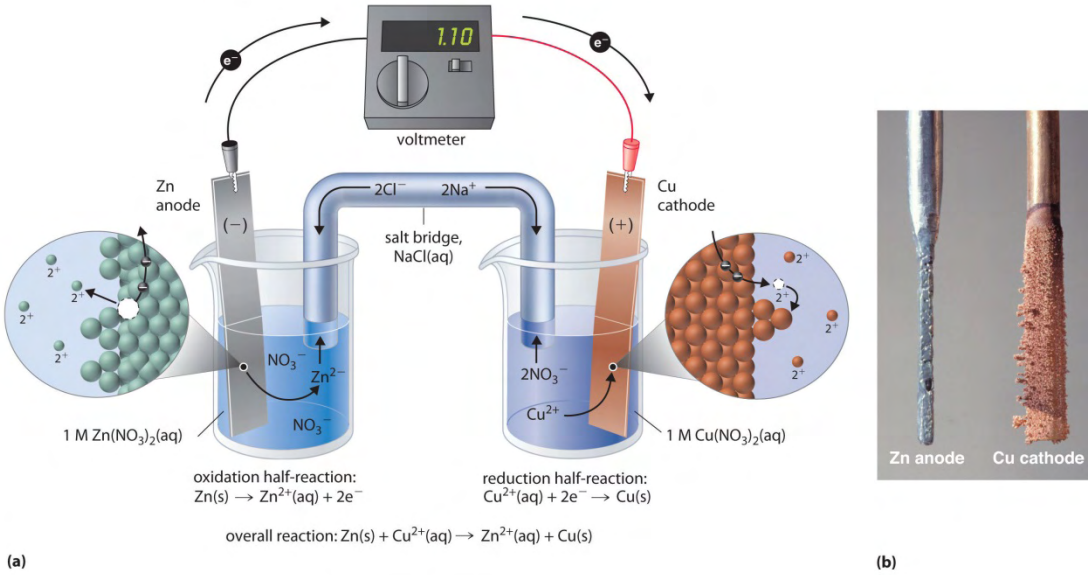

Figure 1.2. a) Complete arrangement of a Daniell cell, b) Anode and cathode as a result of redox reaction[20].

The oxidation of Zn(s) into Zn^{2+} and the reduction of Cu^{2+} to Cu(s) occur spontaneously. In other words, the redox reaction between Zn and Cu^{2+} is spontaneous. This is due to the difference in potential energy between the two substances. The difference in potential energy between the anode and cathode dictates the direction of electronic movement. Electrons move from areas of higher potential energy to areas of lower potential energy. In this case, the anode has a higher potential energy, so the electrons move from anode to cathode. The potential difference between the two electrodes is measured in units of volts. One volt (V) is the potential difference necessary to generate a charge of 1 coulomb (C) from 1 joule (J) of energy. From this aspect, a voltmeter can be used to measure the difference in electrical potential between the two compartments.

Opening the switch that connects the wires to the anode and the cathode prevents a current from flowing, so chemical reactions cannot take place. With the switch closed, however, the external circuit is closed, and an electric current can flow from the anode to the cathode. Therefore, the potential (E_{cell}) of the cell is the difference in electrical potential between the two half-reactions and is related to the energy needed to move a charged particle in an electric field. As the electrons from

the oxidation half-reaction are released at the anode, the anode in a galvanic cell is negatively charged. On the other hand, the cathode, which attracts electrons, is positively charged. The potential (E_{cell}) of the cell, would be analyzed in detail in the following chapter regarding fuel cells.[18, 20]

Finally, there is a great variety of applications which are based on the aforesaid electrochemical processes like the coating of objects[22, 23] with metals or metal oxides through electro-deposition and the detection of alcohol in drunk drivers through the redox reaction of ethanol. Additionally, the generation of chemical energy through photosynthesis is inherently an electrochemical process, as it leads to the production of metals like aluminum and titanium from their ores. Moreover, certain diabetes blood sugar meters measure the amount of glucose in the blood through its redox potential. There is also a wide range of new emerging technologies such as fuel cells, large format lithium ion batteries, electrochemical reactors and super-capacitors that are lately becoming commercial[24]. Electrochemistry has also important applications in the food industry, like the assessment of food/package interactions[25], the analysis of milk composition[26], the characterization and the determination of the freezing end-point of ice-cream mixes, the determination of free acidity in olive oil, and so on.

CHAPTER II

2 FUEL CELLS

Abstract

In the present chapter, the technological breakthrough of fuel cells is presented. Basic principles as well as the main types of fuel cells are analyzed thoroughly. Thermodynamic analysis and electrochemical kinetics are also taken under consideration. Additionally, the applications of a fuel cell are demonstrated. Advantages and disadvantages are also discussed.

2.1 Historical Review

The technological breakthrough of the fuel cells counts back to the 19th century. Welsh physicist Sir William Robert Grove (1811-1896) anticipated the general theory of the conservation of energy and was the pioneer of fuel cell technology. He used a combination of sheet iron, copper and porcelain plates, and a solution of sulfate of copper and dilute acid. He started to observe a low production of voltage, so he decided to connect several voltaic cells in a row as a stack in order to create the so-called "gas battery" *(Figure 1).* Although, many scientists adopted this theory and achieved to update it, Grove is still supposed to be the "father" of the fuel cell novelty[27].

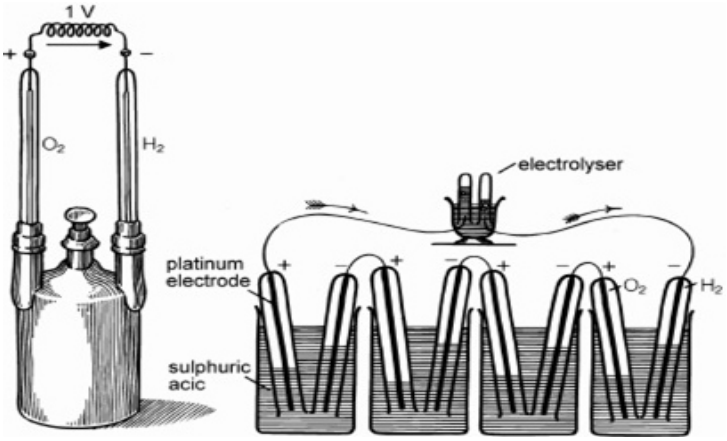

Figure 2.1. Grove's "gas-battery" [28]

In modern days, the NASA was searching for an alternative way of energy to support their space missions. Firstly, they tried to use conventional means of fuel such as batteries, nuclear energy and solar energy. Nevertheless, all these ways were rejected due to overweight cargo (batteries), economical issues (solar energy) and nuclear waste. Fuel cells technology was identified to be a possible solution to their problem so NASA's researchers were immediately assigned to work on this and make it feasible. This led to the invention of the first proton exchange membrane fuel cell (PEM)[27].

The commercialization of the fuel cell technology practically started in the year 1993 when Ballard Vehicle Industry (Canada) manufactured the first fuel cell-powered car. Two years later Daimler-Benz followed by manufacturing a similar but more efficient vehicle. In recent years, fuel cell technology can be found on a wide variety of applications such as hospitals and institutes power supplies and many industries.

2.2 Basic Principles

Fuel cell is an electrochemical device which is able to convert the chemical energy of a conventional fuel (such as hydrogen, methane etc.) directly to electrical power (continuous current). Practically, internal combustion is being replaced by a more efficient and non-polluting energy source.

A typical fuel cell *(Figure 2)* consists of three main parts, two porous electrodes and an electrolyte. At the negative electrode or anode, a fuel such as hydrogen is being oxidized, while at the positive electrode or cathode, oxygen is reduced. Electrodes are connected with an external circuit. Anode is supplied with hydrogen whereas cathode is supplied with oxygen. At this point, an exothermic reaction is taking place as well as water (H_2O) production. Firstly, when the hydrogen reaches the anode, chemical bonds break which leads to the separation of protons and electrons. The electrolyte blocks the electrons and allows the ions (protons) to flow towards the cathode. There, ions and oxygen molecules react with the electrons, which arrive through the external circuit, and produce water with a simultaneously dissipation of heat. Throughout the whole reaction, electrical energy equilibrium should be balanced between the electrical load of the ions of the electrolyte and the flow of the electrons. The overall reaction can be described by the following equations:

- Anode: $H_2 \rightarrow 2H^+ + 2e^-$ (2.1)

- Cathode: $2H^+ + \frac{1}{2}O_2 + 2e^- \rightarrow H_2O$ (2.2)

- Overall: $H_2 + \frac{1}{2}O_2 \rightarrow H_2O$ (2.3)

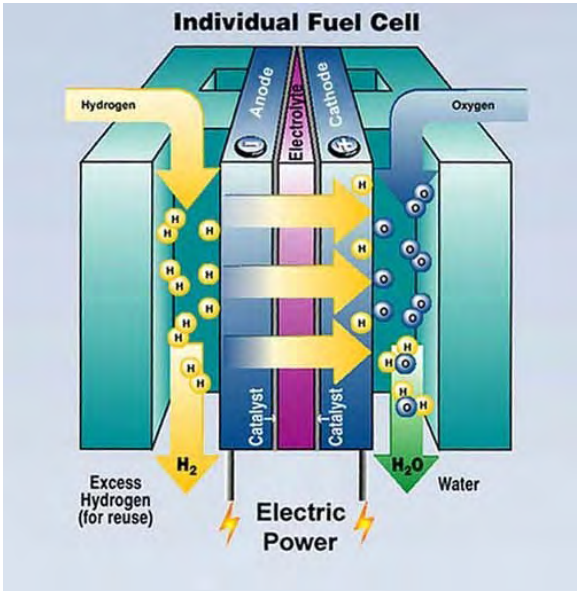

Figure 2.2. A typical Fuel Cell [28]

The choice of the electrolyte is a matter of great importance. The main characteristic of an electrolyte that is taken under consideration is the high ionic conductivity. Moreover, low permeability is advised in order to prevent hydrogen and oxygen from mixing. A short-circuit phenomenon should be avoided, so poor electron conductivity must be ensured. In addition, fuel cell must be chemical stable in a wide range of operating conditions in order to be flexible and able to resist to mechanical stresses. Finally, the ionic conductivity of the electrolyte depends on the values of the temperature; this explains the variety of electrolyte's material.

The electrodes of a fuel cell are of equal importance to the general operating system. They consist of a thin laminate of porous material on which catalyst has been coated with various techniques and accelerates chemical reactions. Ionic and electronically conductive materials should be chosen for the formation of the electrodes. They should also be electrochemically active and stable in both reducing and oxidizing atmosphere[28].

2.3 Thermodynamic Analysis

During the entire process of a fuel cell activity the temperature remains almost constant because it is approximately considered as an isothermal process. Most of the chemical energy of the reactants is converted into electrical, since it is not consumed for the rise of the temperature. This proves that fuel cells do not abide by the law of Carnot, the theoretically maximum temperature, like conventional thermal machines do.

Thermal efficiency of a conventional thermal machine is given by the following equation:

$$\eta_{th} = W_{net} / Q_{in} \qquad (2.4)$$

where W_{net} is the value of the network produced and Q_{in} is the total of the energy provided by the fuel.

The maximum theoretically thermal efficiency of a thermal machine is determined by the reversible cycle of Carnot:

$$\eta_{thCarnot}=1-(T_L / T_H) \qquad (2.5)$$

where T_L , T_H are the values of the lowest and the highest temperature respectively.

All conventional thermal machines cannot overcome the theoretically maximum value of Carnot due to irreversibilities during the combustion and frictions of the mobile parts of the machine. On the opposite, fuel cells do not consist of mobile parts and, since the process is isothermal, thermal efficiency should be greater than the conventional.

In a fuel cell, maximum network $W_{max, cell}$ is given by the following:

$$W_{max, cell} = - \Delta G \quad (2.6)$$

where ΔG shows the change of the free energy Gibbs between the products and the reactants.

The electrical work, W_{cell}, which is produced by the movement of the electrons due to the potential difference, E, between the two electrodes is given by the following:

$$W_{cell} = n_e * F * E \quad (2.7)$$

where n_e is the number of moving electrons per mol and F is the constant of Faraday (F=96484.6 Cb/mol)

Thermal efficiency of a cell is derived from the above equations and is given by:

$$\eta_{th} = n_e * F * E / HHV \quad (2.8)$$

where HHV is the higher calorific value of the fuel.

Moreover, maximum thermal efficiency of a cell derives from the equation (2.8) by replacing potential, E, with the open circuit voltage, E^o, (known, also, as electromotive force) resulting in a state of equilibrium when there is no power output.

$$\eta_{th} = n_e * F * E^o / HHV \quad (2.9)$$

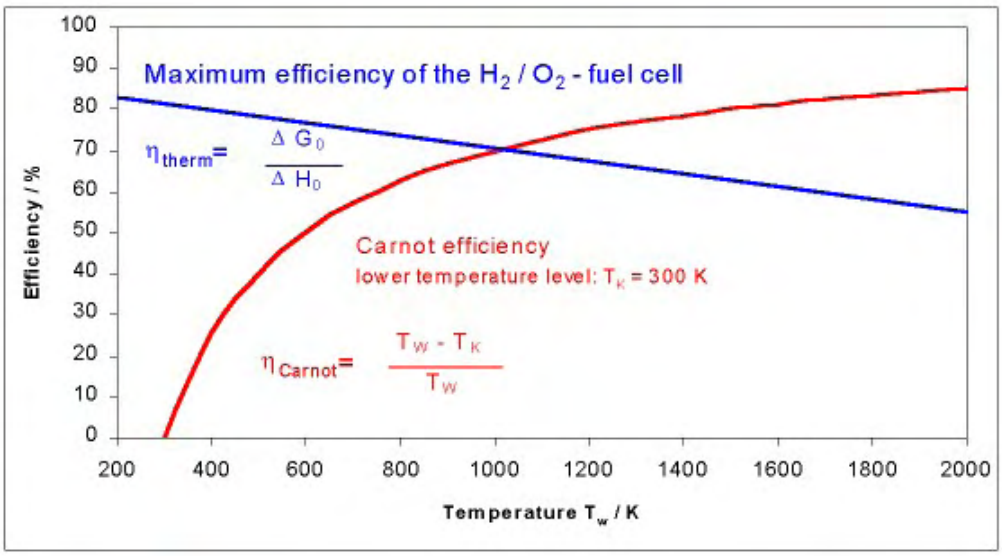

Figure 2.3. Thermodynamic efficiency for fuel cells and Carnot efficiency for heat engine[29]

The above equations are developed based on the first law of thermodynamics. However, by taking under consideration the second law of thermodynamics, thermal efficiency indicates the percentage of net work during the process of energy production due to irreversibility. Essentially, it depicts the difference between the actual and the ideal device.

According to the second law of thermodynamics, the thermal efficiency of a fuel cell is:

$$\eta_{cell,II} = W_{actual} / W_{ideal} = E / E^{o} \qquad (2.10)$$

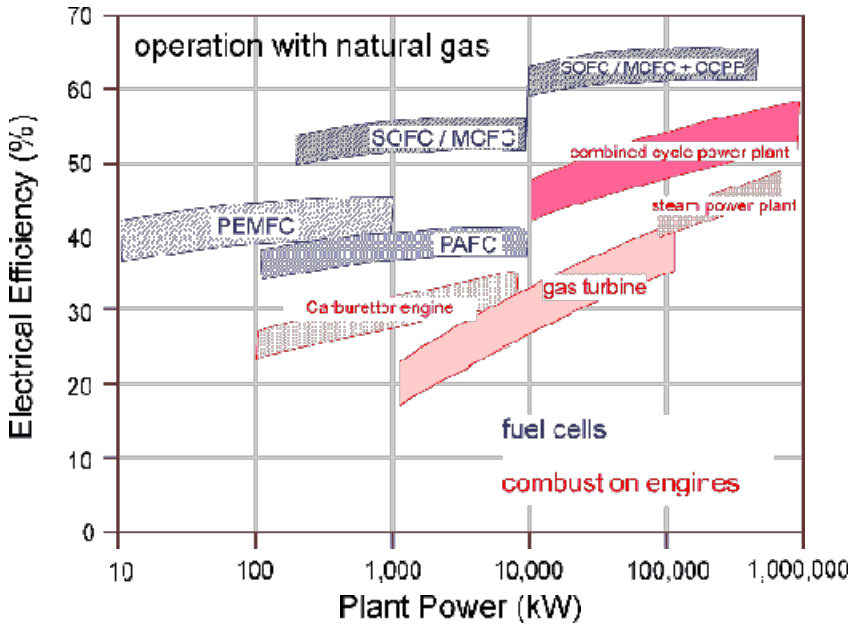

Figure 2.4. Comparison of thermal efficiency between conventional thermal machines and fuel cells

In *Figure 3*, the thermodynamic efficiency of a fuel cell as well as thermal efficiency of Carnot cycle is depicted and *Figure 4* illustrates a comparison of the thermal efficiency between commonly used thermal machines and fuel cells.[28]

2.4 Electrochemical Kinetics

Electrochemical reactions can be divided into two different types of reactions: cathodic and anodic reactions. In cathodic reactions, the electrons flow from cathode to anode, causing cathodic current, I_c. On the other hand, in anodic reactions there is a production of anodic current, I_a, due to the electrons discharged from the electro-active substances on anode, causing the oxidation of this electrode.

The potential, E, which is generated by a fuel cell during the accomplishment of the reaction:

$$aA + bB \rightarrow mM + nN \qquad (2.11)$$

is given by the Nernst equation, in honor of Walther Nernst(1864-1941), a German physical chemist who formulated it first, and is:

$$E = E_o - (RT / n_eF) \ln(P_M^m P_N^n / P_A^a P_B^b) \qquad (2.12)$$

where E_o is the open circuit voltage , which is the maximum potential produced by the cell in equilibrium, P_i^j are the partial pressures of the reactants and the products, R is the universal gas constant (R= 8.314472(15) J/Kmol) and T is the temperature in Kelvins. The potential difference E- E_o is called overpotential. It is denoted byηand distinguished in anodic (positive) overpotential and cathodic (negative) overpotential, depending on which electrode is displayed.

The current density, I, can be expressed as overpotential, through Butler-Volmer equation, which is a fundamental relationship of electrochemical kinetics and is given by the following equation:

$$I= I_o [\exp(-n\beta F\eta/RT) – \exp (n(1-\beta) F\eta /RT)] \qquad (2.13)$$

Where β is the charge transfer coefficient($0<\beta<1$), n is the number of electrons involved in the electrode reaction, η is the overpotential and I_o is the exchange current density.

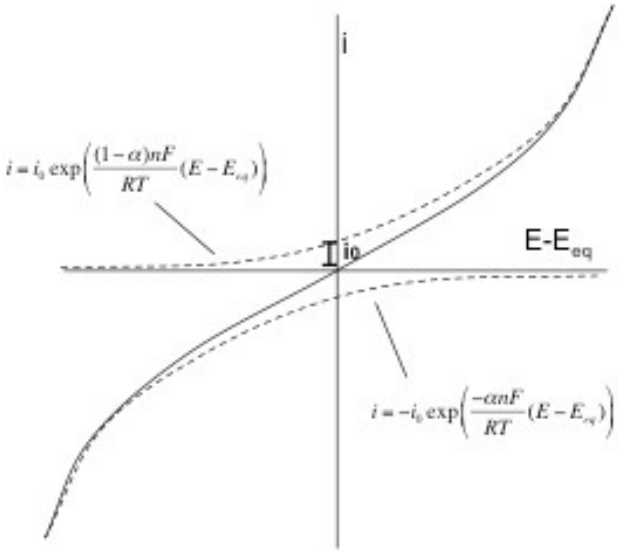

Figure 2.5. Rate of electron transfer vs. potential in Butler-Volmer relationship for reversible reaction

- For low values of overpotential(η< 10 mV), the current density is transformed into the following equalization:

$$I = (I_o\, n\, F\, \eta)/ RT \qquad (2.14)$$

- For high values of overpotential (η>120 mV), equation (2.13) can be satisfactorily approached by the Tafel equation:

$$\eta = \alpha + b \log I$$

where a, b have different values for anodic and cathodic overpotential,

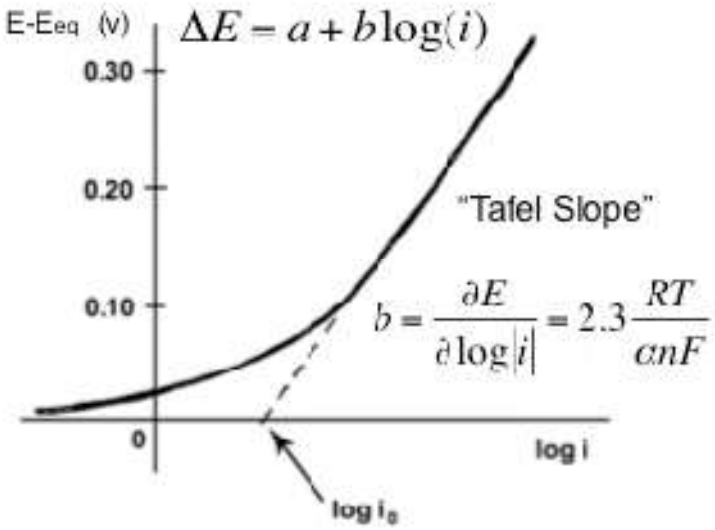

Figure 2.6. Rate of electron transfer vs. potential in Tafel relationship for reaction far from equilibrium

and more specifically:

- For cathodic overpotential:

$$\alpha = 2.303\ RT \log I_o / a\ n\ F \text{ and } b = -2.303\ RT \log I_o / a\ n\ F \qquad (2.15)$$

- For anodic overpotential:

$$\alpha = -2.303\ RT \log I_o / (1-a)\ n\ F \text{ and } b = 2.303\ RT \log I_o / (1-a)\ n\ F \qquad (2.16)$$

The Tafel equation indicates that the low kinetics of the reaction in a low temperature fuel cell contributes to the open circuit voltage E_o, in a quantity:

$$E - E_o \approx b \log I_o \qquad (2.17)$$

2.5 The phenomenon of overpotential

Generally, the deviation from the reversible potential (or open circuit voltage, OCV) is called overpotential and it derives from various irreversibilities during fuel cell operation. As it was mentioned above, overpotential is given from the following equation:

$$\eta = E - E_o \qquad (2.18)$$

Moreover, overpotential is characterized as anodic, when the current density is positive ($E>E_o$), whereas when the current density is negative ($E<E_o$), it is called cathodic.

Overpotential can, also, be divided into four main types, depending on the kind of irreversibility, and more specifically into:

1. *Activation Overpotential*(η_{act})

This kind of overpotential is associated directly not only with the current density flowing through the electrode, but also with the velocity of the electrochemical reaction. It is also called polarization of the electrode as a result of the slow rate of the half-reaction, which is carried out on the electrode's surface.

The slow kinetics of the electrodes has a special effect on activation overpotential mainly in low temperature fuel cells. This type of overpotential is measured by the following equation:

$$\eta_{act} = (RT/ anF) \ln(I_o/I) \qquad (2.19)$$

where α is the transport coefficient expressing the ratio of the overpotential which refers to the reaction, and I_o is the exchange current density.

2. *Ohmic or Resistance Overpotential*(η_{ohm})

The resistance which is appeared in the flow of electrons due to the electrode's material, as well as the resistance to the ion movement through the electrolyte, is the main reason of this form of overpotential. It is proportionate to the current density and follows a linear dependence of it. This type of overpotential is measured by the following equation:

$$\eta_{ohm}=I\,R_{ohm} \qquad (2.20)$$

where R_{ohm} is the ohmic resistance of the surface, which includes terms concerning not only the electrolyte, but also the electrodes, the current collectors and the driver-cables that are parts of the system.

The Ohmic Overpotential will be reduced, if electrode's thickness is decreased or if the use of electrodes with high conductivity is preferred. Furthermore, an appropriate design of the interface devices is necessary for the depletion of the "junction" issues.

3. *Concentration Overpotential* (η_{conc})

The mass transfer which occurs during the operation of a fuel cell is carried out by diffusion, convection or physical separation. The term of physical separation is negligible when there is no electric field, whereas the term of convection is null when the process is performed under steady-state conditions.

The Concentration Overpotential indicates mass diffusion and depends on cell's geometry. It is determined by the flow rate of the reactants in the electrolyte as well as the removal rate of the reaction products; it takes place on both anode and cathode. The higher the current density is applied to the fuel cell, the weaker the reactants' zone is. Thus, at high current density levels, the overpotential due to mass diffusion is greater than the lowest levels.

4. *Crossover Overpotential*(η_{cross})

This last kind of overpotential is due to the loss of fuel through the electrolyte. As it was mentioned above, electrolyte works as an ionic conductor. Inevitably, a small amount of fuel permeates through the electrolyte and effects considerably the open circuit voltage, especially in low temperature fuel cells[30, 31].

The typical behavior of a fuel cell is shown in *Figure 7*. The total overpotential derives from the sum of the aforesaid four types of overpotential, and is given by the following equation:

$$\eta= \eta_{act} + \eta_{ohm} + \eta_{conc} + \eta_{cross} \qquad (2.21)$$

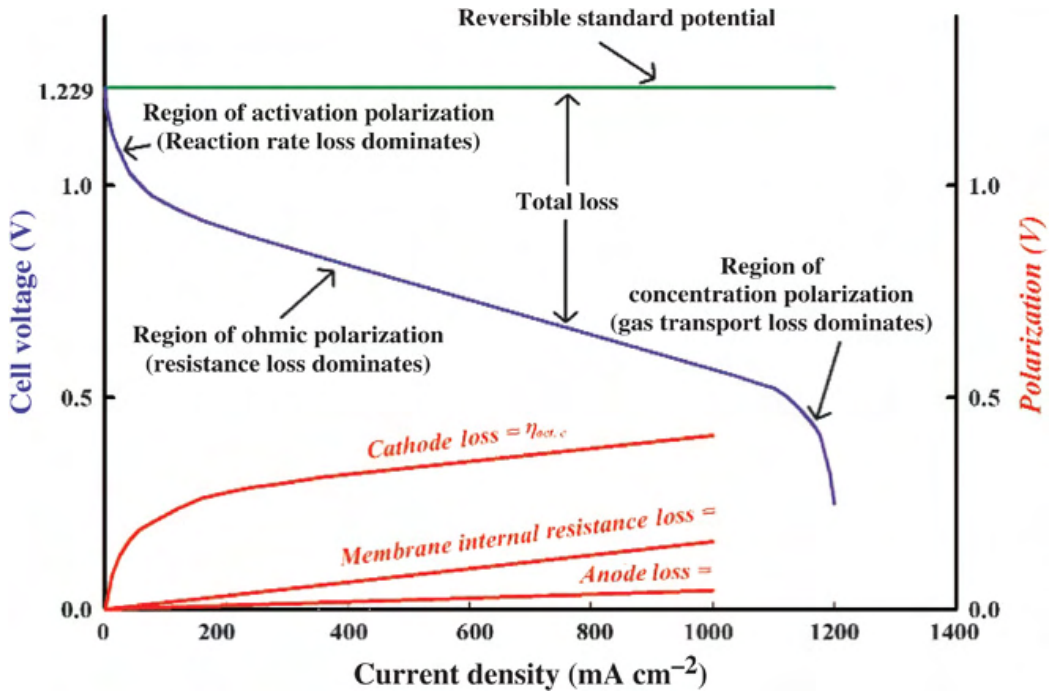

Figure 2.7. Polarization curve of a fuel cell [32]

2.6 Fuel Cell Potential

The thermal efficiency of a fuel cell is determined by the potential which is measured at the cell output and is a function either of the current density or the overpotential curve. The measured potential due to overpotential equals the algebraic sum of the equilibrium potential E_o, the potential which refers to losses along the electrolyte E_l, the total developing overpotential, and is given by the following equation:

$$E = E_o - E_l - \eta_{act} - \eta_{ohm} - \eta_{conc} - \eta_{cross} \quad (2.22)$$

The equilibrium potential is a result of thermodynamic analysis of the reaction occurring at the fuel cell. It is determined by the Gibbs free energy and measured by the following equalizations:

$$E_o = - \Delta G / n F \quad (2.23)$$

and

$$\Delta G = \Delta G°(T) + RT \ln (P_{H2} P^{1/2}_{O2} / P_{H2O}) \quad (2.24)$$

where $\Delta G°$ is the Gibbs free energy of the reaction when all substances are in standard conditions, while the terms of pressures in the right side of the Equation 2.24 refer to the actual pressures of the substances at the operating conditions of the fuel

cell. In open circuit voltage conditions the measured potential is identified with Nernst's electromotive force (EMF).

2.7 Different Types of Fuel Cells

The classification of fuel cells is based on the type of the electrolyte that is used. However, the kind of the electrolyte defines, also, other aspects of the cell, such as the operating temperature, the type of catalyst as well as the susceptibility to poisoning. Thus, there are significant differences among the types of fuel cells. Most important of these will be presented as it follows:

2.7.1 Alkaline Fuel Cell (AFC)

Alkaline Fuel Cells, also known as Bacon Fuel Cells due to British inventor Francis Thomas Bacon (1904-1992), are considered to be the first modern fuel cells. They were created in 1960 in order to provide an alternative way of energy for space applications. They are the simplest form of low temperature fuel cell technology both in terms of design and operation(*Figure 8*). Hydrogen (H_2) is used as fuel and the electrolyte is Potassium Hydroxide solution (KOH) either in high concentration (85 % w.t.) for operation at relatively high temperature (T~250°C) or in low concentration (30-50 % w.t.) for operation at temperatures lower than 120 °C. The standard operating conditions of AFCs are 70 °C and solution KOH in concentration 30% w.t. In case of room temperature, AFCs operate properly with a decrease of their nominal efficiency to 50 %. The main reactions that are taking place in an AFC are the following:

- Anode : $H_2 + 2(OH)^- \rightarrow 2\,H_2O + 2e^-$ (2.25)
- Cathode : $\frac{1}{2}\,O_2 + H_2O + 2e^- \rightarrow 2(OH)^-$ (2.26)
- Overall : $H_2 + \frac{1}{2}\,O_2 \rightarrow H_2O$ (2.27)

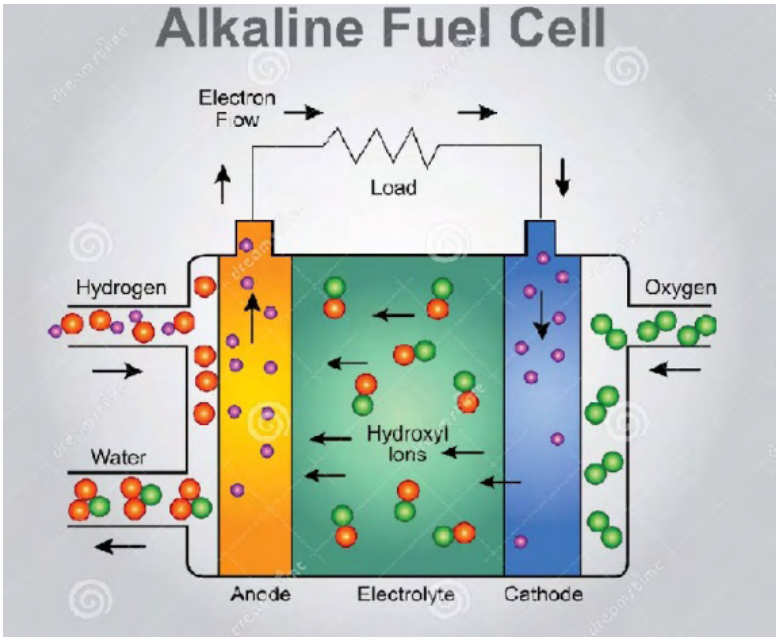

Figure 2.8. A typical depiction of an Alkaline Fuel Cell (AFC) [32]

Generally, AFCs have higher efficiency in combustion of H_2 with O_2 than any other fuel cell as well as greater flexibility in the utilization of the catalysts. The most commonly used catalysts are nickel (anode) and platinum (cathode). On the other hand, there are some serious drawbacks concerning AFCs. More specifically, they are unable to operate via air as an oxidizing agent while undiluted K_2CO_3 is formed at the cathode. Moreover, they show high susceptibility to CO_2 poisoning. Therefore, the removal of CO_2 which is a product of the fuels derived from reforming as well as the H_2O produced from the overall reaction, are crucial issues for optimal function of AFCs. Otherwise, water remains in KOH, dilutes it and leads to lower efficiency of the cell.

2.7.2 Phosphoric Acid Fuel Cell (PAFC)

PAFC are the first type of fuel cells ever to be commercialized. They were developed in the mid-60s and they have significantly improved in stability, performance and cost. These developments have made the PAFC a reliable candidate for early stationary applications. PAFC operate between 150° C and 200° C. Phosphoric acid is used as an electrolyte and hydrogen and oxygen are used as fuels in anode and cathode respectively. Protons pass through electrolyte from anode to cathode (*Figure 9*). Electrons produced from the separation of hydrogen travel

through an external electrical circuit, providing electrical current to the system, and finally arrive at the cathode. There, in combination with protons from the electrolyte and oxygen molecules they form water which is released from the cell. Platinum catalyst speeds up the reaction. The main reactions which take place are the following:

- Anode: $2H_2 \rightarrow 4H^+ + 4e^-$ (2.28)
- Cathode: $O_2(g) + 4H^+ + 4e^- \rightarrow 2H_2O$ (2.29)
- Overall: $2H_2 + O_2 \rightarrow 2H_2O$ (2.30)

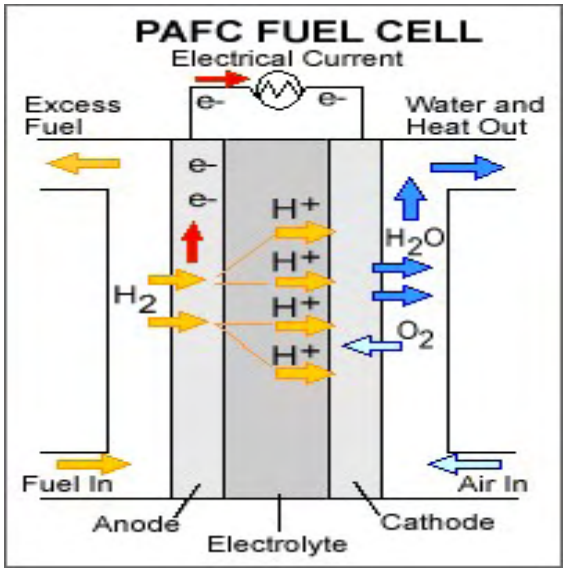

Figure 2.9. Scheme of a typical Phosphoric Acid Fuel Cell [32]

PAFC efficiency ranges from 40% to 50%. In case of cogeneration through heat waste, the efficiency can reach 80%. PAFC are capable of producing up to 200 kW and support, from the energy spectrum, power plants up to 11 MW. A vital advantage of a PAFC is the resistance to the "poisoning" of CO as the can endure a CO concentration up to 1.5% at 200° C. Another important advantage is that phosphoric acid can overcome the boiling temperature and still operate properly, which is a restriction to other acid catalysts that require water for their conductivity. However, materials that can resist corrosion are required.

2.7.3 Proton Exchange Membrane Fuel Cell (PEMFC)

PEM fuel cells, also known as polymer electrolyte membrane, are a type of fuel cells being developed for transport applications as well as for stationary and portable fuel cells applications. They are a leading candidate to replace the aging alkaline fuel cell technology, which was used in the Space Shuttle. They operate with a polymeric electrolyte shaped as a thin and permeable sheet*(Figure 10)*. This membrane can function at 80° C. Platinum is used as a catalyst in both sides of the electrolyte in order to accelerate the reaction. Positively charged hydrogen ions are diffused through a porous membrane (which blocks electrons and heavy gases from passing through) from anode to cathode. Electrons follow a similar route in which the membrane is replaced by an external circuit, providing electrical power. Water is produced at the cathode due to the reaction of electrons, protons and oxygen molecules. The main reactions are the following:

- Anode: $H_2 \rightarrow 2H^+ + 2e^-$ (2.31)
- Cathode: $\frac{1}{2}O_2 + 2H^+ + 2e^- \rightarrow H_2O$ (2.32)
- Overall: $H_2 + \frac{1}{2}O_2 \rightarrow H_2O$ (2.33)

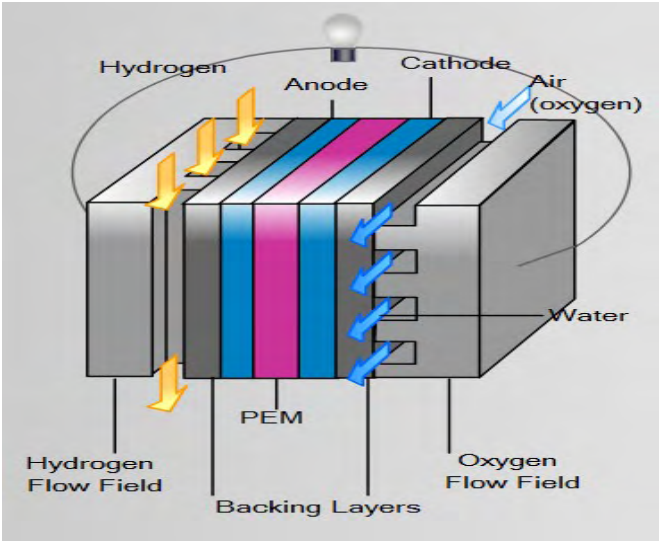

Figure 2.10. Depiction of a typical Proton Exchange Membrane Fuel Cell [32]

PEM fuel cell efficiency ranges from 40% to 50%. An external reformer for the conversion of fuels (methanol or gasoline to hydrogen) is recommended. Currently, PEM fuel cells operate producing up to 250 kW.

2.7.4 Solid Oxide Fuel Cell (SOFC)

Solid Oxide fuel cells function at high temperatures. In late 1950s, researchers, on their attempt to create a device which could operate at high temperatures with a solid electrolyte, discovered this type of cell. A typical SOFC uses a solid ceramic electrolyte, instead of liquid, which functions at temperatures between 400° C and 1000° C. Although, a lot of combinations of oxides have been used as electrolytes, the preferred oxides consist of a mixture between zirconium (yttrium stabilized zirconia) and calcium which form a crystal lattice. The solid electrolyte is coated from both sides with specialized materials used as electrodes (*Figure 11*).

At this high temperature, oxygen anions pass through the crystal lattice. During the supply of the fuel (hydrogen in gaseous form) through the anode, a flow of oxygen anions pass through the electrolyte in order to oxidize the fuel. Oxygen is supplied at the cathode. Electrons produced at the anode flow through an external circuit to the cathode, providing electrical power. The main reactions of this operation are the following:

- Anode: $2H_2 + 2O^{2-} \rightarrow 2H_2O + 4e^-$ (2.34)
- Cathode: $O_2 + 4e^- \rightarrow 2O^{2-}$ (2.35)
- Overall: $2H_2 + O_2 \rightarrow 2H_2O$ (2.36)

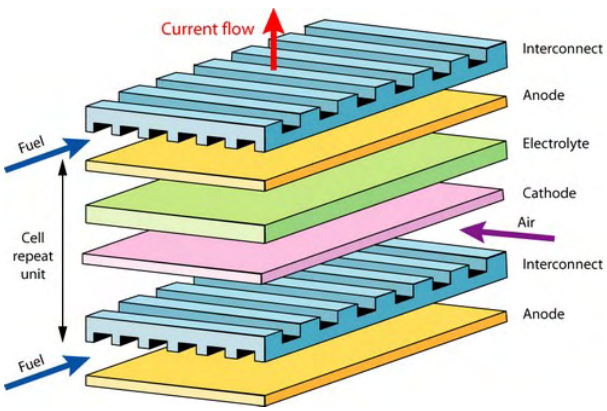

Figure 2.11. A typical flat plate Solid Oxide Fuel Cell [32]

SOFC efficiency reaches up to 60% and since they operate at such high temperature no reformer is required to produce pure hydrogen from the fuel.

2.7.5 Molten Carbonate Fuel Cells (MCFC)

MC fuel cells are currently being developed for natural gas, bio-gas and coal based power plants for electrical utility, industrial and military applications. In this type of fuel cells, carbonates play the role of the electrolyte *(Figure 12)*. At a temperature of 650° C, carbonates melt and lead the carbonate ions (CO_3^-) from cathode to anode. At the anode, hydrogen molecules react with the ions in order to produce water, carbon dioxide and electrons. These electrons travel through an external circuit to the cathode, providing electrical power. There, oxygen and carbon dioxide molecules produced at the anode react with the electrons forming carbonate ions which refill the electrolyte and transfer the electrical current through the cell. The main reactions of the procedure are the following:

- Anode: $CO_3^{2-} + H_2 \rightarrow H_2O + CO_2 + 2e^-$ (2.37)
- Cathode: $CO_2 + \frac{1}{2}O_2 + 2e^- \rightarrow CO_3^{2-}$ (2.38)
- Overall: $H_2(g) + \frac{1}{2}O_2(g) + CO_2\,(\text{cathode}) \rightarrow H_2O(g) + CO_2\,(\text{anode})$ (2.39)

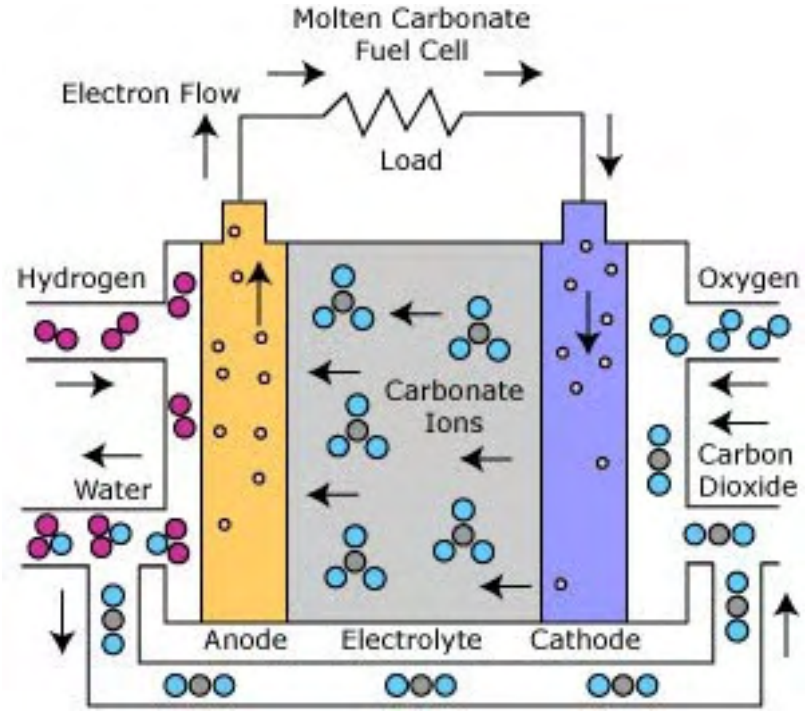

Figure 2.12. A typical depiction of a Molten Carbonate Fuel Cell [32]

High-temperature MCFC has the capability of extracting hydrogen from a variety of fuels using either internal or external reformer. They are also less prone to being "poisoned" from carbon monoxide than other cells functioning at a lower

temperature. MCFC work more efficiently using nickel catalysts rather than platinum catalysts. Their efficiency reaches up to 60%, but in case of cogeneration (through heat waste) it can count up to 80%. So far, units consisting of MCFCs produce up to 100MW.

Two major disadvantages of MCFC compared to SOFC are, firstly, the complexity in their operation with the electrolyte and, secondly, deriving from the chemical reaction that takes place in MCFC. Carbonate ions from the electrolyte are consumed in the anode reaction, making it necessary to balance with the injection of carbon dioxide into the cathode.

Except for the aforesaid types of fuel cells, it is crucial to mention some other types less widespread such as Direct Methanol Fuel Cell (DMFC), Regenerative Fuel Cell (RFC), Zinc Air Fuel Cell (ZAFC), Proton Ceramic Fuel Cell (PCFC) and Microbial Fuel Cell (MFC). [28, 30, 31]

2.8 Applications of Fuel Cells

Fuel cells can be used in the portable, transportation or stationary sectors. They are very useful as sources of power generation for remote areas such as spacecraft and satellites, remote meteorological stations, large energy parks, rural areas and some military applications. For example, a fuel cell which consumes hydrogen can be compact and light, having no moving parts. This fact in combination with the absence of the combustion process, can lead to 99,999% reliability, under ideal conditions.

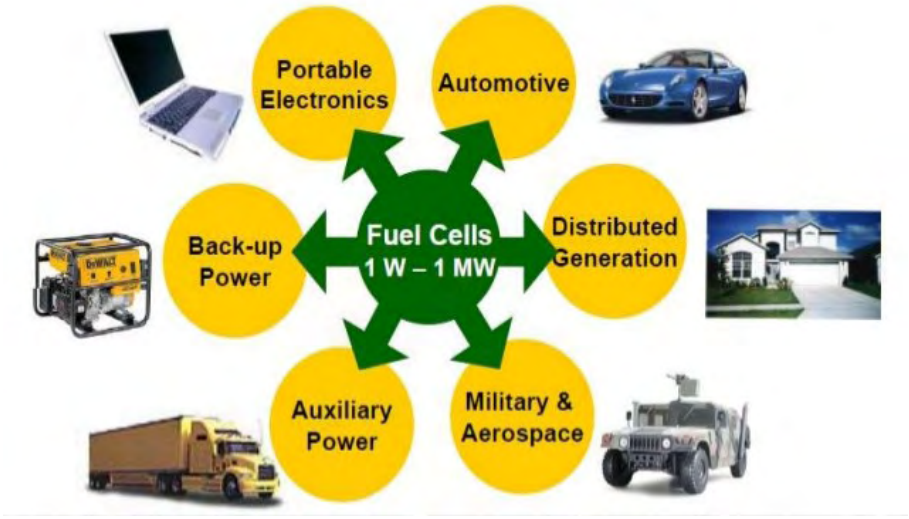

Figure 2.13. Basic applications of Fuel Cell [32]

Micro-combined heat systems and power systems like fuel cells for home applications and cogeneration systems for buildings and industries are in a mass production phase. Production power plants using fuel cells as power generators produce stable electrical power as well as steam from heat waste. The minimum degree of efficiency of fuel cells in order to convert the fuel into electricity is of 15-20%, due to the high percentage of energy converted into heat. The combination of fuel cell's thermal and electrical power, although it remains below 100%, it is about 80%, as a result of part of the heat is lost with the fuel gas. However, in terms of exergy the process is inadequate and could be more efficient by increasing the electrical output produced and using it in order to operate a heat pump.

PAFCs include most of the existing cogeneration units worldwide, providing a power output of up to 90% (35-50% is electrical power and the rest is of the exploitation of thermal power). Moreover, in the aforesaid applications MCFCs can be used as well as SOFCs[31, 32].

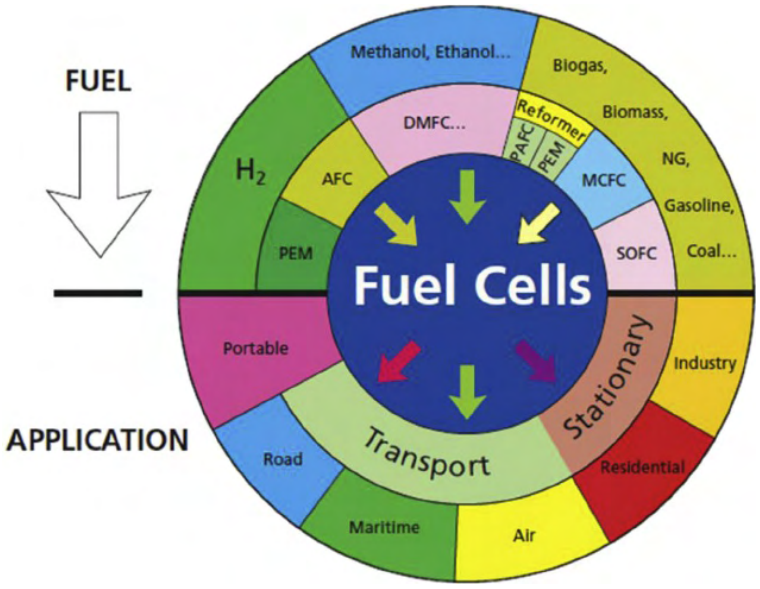

Figure 2.14. An overall depiction of different utilizations of Fuel Cells [33]

The electrolytic systems can be successful as large-scale energy storage applications, especially in rural areas, since they are unable to store fuel and are based on external storage. However, in this application batteries should be enormous to meet the storage requirements, so fuel cells could be a good choice as they need a larger storage unit, basically cheaper than an electrochemical device (battery).

Table 2.1. Characteristics of each type of fuel cells[1, 33]

Type	Electrolyte	Fuel	Operating Temperature	Typical Stack Size	Efficiency	Typical Applications
Alkaline Fuel Cells (AFCs)	Potassium Hydroxide	Pure Hydrogen	90-200 ºC	10-100 kW	60%	Military Services, Space exploration
Phosphoric Acid Fuel Cells (PAFCs)	Phosphoric Acid	Pure Hydrogen	150-220 ºC	400 kW, 100 kW module	40%	Buses, Trucks, Large Stationary Applications, Distributed Generation
Proton Exchange Membrane Fuel Cells (PEMFCs)	Sulfonic Acid incorporated into a solid membrane	Pure Hydrogen, Methanol	50-100 ºC	1-250 kW	60% transportation, 35% stationary	Backup power, Portable power, Distributed Generation, Transportation, Specialty Vehicles
Solid Oxide Fuel Cells (SOFCs)	Ceramic, Solid Oxide, Zirconia	Most Hydrocarbon Based Fuels	450-1000 ºC	1 kW-2 MW	50-60%	Auxiliary power, Electric utility, Distributed Generation, Small to Large stationary power generation
Molten Carbonate Fuel Cells (MCFCs)	Molten Lithium Carbonate	Most Hydrocarbon Based Fuels	550-700 ºC	300 kW-3 MW, 300 kW module	50-60%	Electric utility, Distributed Generation, Large stationary power generation

2.9 Advantages and Disadvantages

Environmentally friendly operation and high energy efficiency, considerably higher than a conventional machine, make the fuel cell a device with a lot of great advantages. More precisely, most of the advantages are mentioned below[28, 34]:

- High energy conversion efficiency (60~65%) from chemical to electrical using pure hydrogen as a fuel.
- High current density.
- Almost silent operation, except for the noises of created by regional support systems.
- Zero contribution to the greenhouse effect, and generally, to the environmental pollution due to low to negligible pollutant emissions from their operation.
- Mobility in their construction, since there are no moving parts.
- Reliability of 99% greater than conventional machines (Power density increased 10 times, while the cost reduced 10 times).
- Unlimited lifetime.
- Wide variety of fuels except for hydrogen (methane, methanol, ethanol).
- Wide range of operating temperatures (80° C to 1000° C).
- Safety in their function except for the usage of fuels involving known risks.

Nevertheless, there are still many disadvantages concerning their utility, associated with their entrance to the field of trade. These drawbacks are summarized in the following:

- High manufacturing cost and in most cases prohibitive for commercial use.
- Expensive process for the production of hydrogen and, in the case of reforming of natural gas, high concentration of CO_2 released to the environment which contributes to global warming.
- Substituting of the conventional power generating facilities with fuel cells will cost millions of dollars.
- Hydrogen storage is probably one of the most important disadvantage of a fuel cell due to its high cost and risky means of storage.

CHAPTER III

3 PEM FUEL CELLS

Abstract

In the present chapter, the main components of a PEM fuel cell (membrane, electrodes, gas diffusion layer and bipolar plates) are reviewed. A thorough investigation of a PEM fuel cell in accordance with the anatomy of these devices is being reported.

3.1 Anatomy of PEM Fuel Cell

The main components of a PEM fuel cell are a polymeric electrolyte in the form of a thin membrane and two porous electrodes located on the two sides of the membrane. Polymeric electrolyte displays proton conductivity. Both electrodes are porous in order to help the reactant gasses to reach the interface between electrodes and membrane. On this interface, electrochemical reactions take place on the catalytic layers (catalyst's surface). Catalytic layers can either be a part of the porous electrode or part of the membrane, depending on its manufacture. The multilayer layout membrane, placed between the electrodes is usually called Membrane Electrode Assembly (MEA). MEA is positioned between the two disks (Collector and Separator). The collector is responsible for the accumulation and conductivity of the electrical current and the separator for the division of the gasses from adjacent cells, in case of a stack. Moreover, in a fuel cell stack (multi-cell configuration), the cathode of the first cell is connected to the anode of the next cell. This is the reason they are

called bipolar disks since they provide the way for the flow of the reactants as well as the structural stability[35].

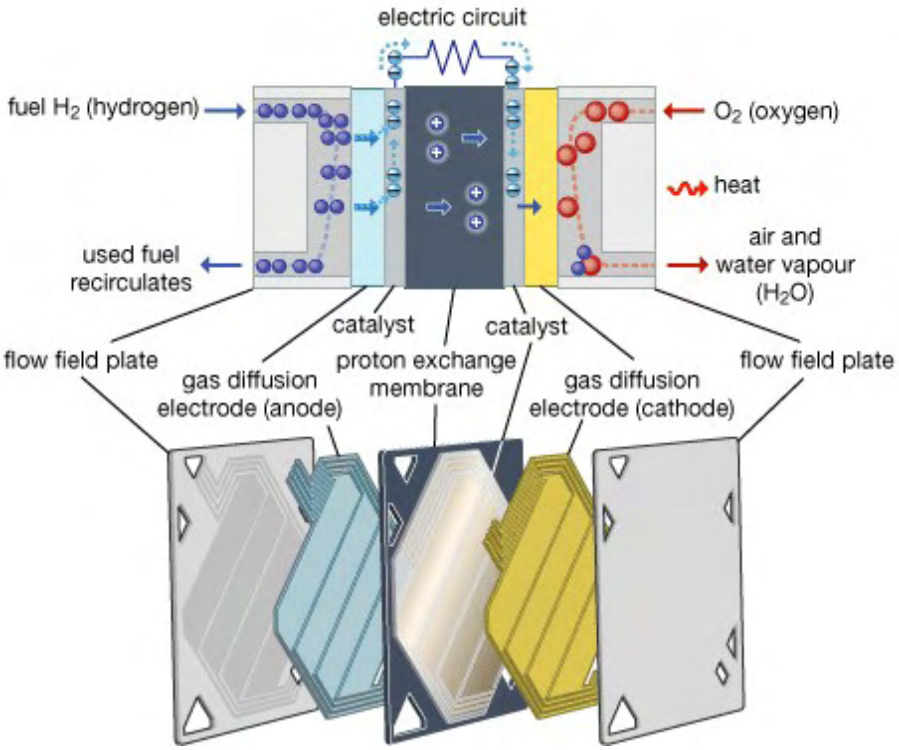

Figure 3.1. Main components of a PEM fuel cell [36]

The procedure of a fuel cell function is described by the following steps:

- The gas flows through the channels of the two electrodes.
- Diffusion of the gas through the porous medium.
- Electrochemical reactions taking place at both anode and cathode.
- Protons transfer through MEA.
- Flow of the electrons through the conductive parts of the cell and an external circuit.
- Production of water taking place at the cathode due to the reaction of descending electrons, protons from the membrane and oxygen molecules.
- At the same time, water is being transported through the membrane due to reverse diffusion and electro-osmosis.
- Heat transfer through solid parts and convection from the reacting gasses and the cooling medium.

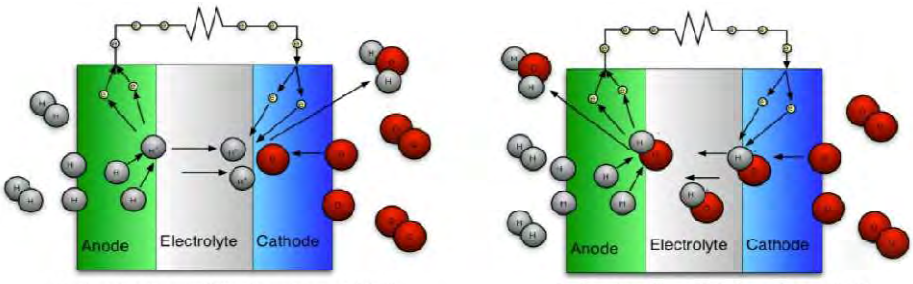

3.2

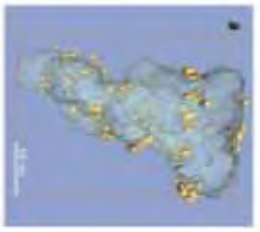

3.3

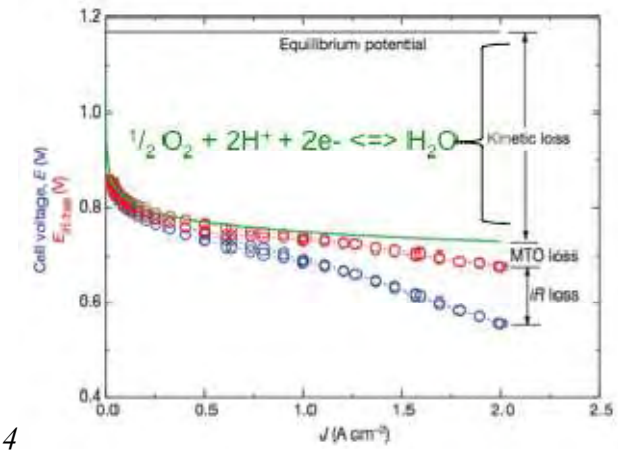

3.4

Figure 3.2. Basic design and electrode reactions for a hydrogen fuel cell

Figure 3.3. Tomographic reconstruction of supported catalyst particles from a fuel cell cathode and model of a typical Pt catalyst nanoparticle[36, 37]

Figure 3.4. Current-voltage performance of a state-of-the-art PEM cell using Pt electro-catalyst electrodes[38]

3.2 Membrane

The vital characteristics of the membrane in order to be considered as an efficient electrolyte are the following:

- High proton conductivity
- Preventing fuel and oxidizing gas from mixing
- Chemically and mechanically stable under the cell's environment.

The material of the polymeric membrane is usually an ionomer perfluorocarbon sulphonic acid (PSA), which is basically a copolymer of tetrafluorethylene (TFE) and a variety of other perfluorosulfonate monomers. The most usual material of the membrane is Nafion®. It is produced by Dupont Industries, and it is based in PSERVE (perflurosulphonylfluoride ethyl-propyl-vinyl ether).

This Teflon-like material is highly hydrophobic while the sulphonic acid is highly hydrophilic. The hydrophilic regions are created around the sulphonated side chains. That is the reason why these materials absorb large quantities of water (in some cases 50% of their weight). The movements of the positive ions within well-hydrated regions make these materials proton conductive.

Nafion® membranes are extrusion products and have a variety of different sizes and thicknesses. The equivalent weight, which is practically a measurement of ionic concentration inside the monomer, in geq^{-1} of a polymer membrane is given by the following equation:

$$EW = 100n + 446 \quad (3.1)$$

Where n is the number of TFE groups on average per PSERVE monomer[32].

3.2.1 Water Uptake

Proton conductivity of a polymer membrane depends on the structure and water content of the membrane. The water content is usually expressed as water grams per grams of polymer dry weight, or as the number of water molecules per sulphonic acid groups, present in the polymer (Equation 3.2).

$$\lambda = N(H_2O) / N(SO_3H) \quad (3.2)$$

The maximum amount of water in the membrane is strongly dependent on the state of the water, used to equilibrate the membrane. Additionally, the amount of water in liquid phase that the membrane can accept depends on the production method and the preparation it has undergone. The quantity of water in gas phase is more important for the fuel cell as the reaction gasses (reductants and oxidants) enter the cell hydrated.

3.2.2 Physical Properties

The amount of water in the membrane leads to volume expansion and dimensional changes, which are vital factors for the design and assembly of the fuel cell.

3.2.3 Proton Conductivity

The most important property of a polymeric membrane used in fuel cells is proton conductivity. Polymer's density in an ionomer membrane of proton conductivity of equivalent weight of 1100 is equal to 1M aqueous sulfuric acid solution. It is noteworthy that proton mobility in a fully hydrated membrane is only a scale lower than the proton mobility in an aqueous sulfuric solution.

Consequently, proton conductivity of a fully hydrated membrane is about 0.1S / cm, at room temperature. Conductivity of a PFSA type membrane depends on the content of water and the operating temperature.

3.2.4 Water Transport

There are numerous mechanisms of water transportation through the polymeric membrane. Water is produced on the cathode as a result of the electrochemical reaction. The water production rate (mol/cm^2*s) is given by:

$$N_{H2O,gen} = i / 2*F \quad (3.3)$$

where i is the current density in A / cm^2 and F is the Faraday constant.

Water is drifted from the anode to the cathode through the electrolyte. This phenomenon is called electro-osmotic transport. The flow of the water due to the electro-osmotic transfer (mol/cm^2 sec):

$$N_{H2O,\,drag} = \xi(\lambda) * i / 2*F \quad (3.4)$$

where ξ is the electro-osmotic transfer factor(mol_{H2O} / proton). Basically, it is factor which depends on the hydration of the membrane.

Water production and electro-osmotic transportation create a great slope of concentration along the membrane. Due to this gradient, a quantity of water diffuses

in the opposite direction to the anode (reverse osmosis).The rate of water diffusion (mol/cm^2 sec) is given by:

$$N_{H2O,\ diff} = D(\lambda) * \Delta c / \Delta z \quad (3.5)$$

where D is the diffusion coefficient of water and $\Delta c / \Delta z$ is the concentration difference (in z direction).

In combination with diffusion due to concentration difference, water can transfer hydraulically, due to pressure difference between anode and cathode. The rate of hydraulic permeation (mol/cm^2 sec) is given by:

$$N_{H2O,\ Hyd} = k_{hyd}\ (\lambda) * \Delta P / \Delta z \quad (3.6)$$

where k_{hyd} is the hydraulic permeability coefficient of the membrane of the water content λ and $\Delta P / \Delta z$ is the pressure gradient along the z direction.

3.2.5 Gas Permeation

The membrane should be impervious in order to prevent the reactants from mixing with other electrochemical reactions. However, given their porous structure, water content and solubility of hydrogen and oxygen in the water, several gasses penetrate the membrane.

Permeability is the product of diffusivity and solubility and it is given by:

$$P_m = D * S \quad (3.7)$$

Since diffusivity is expressed in cm^2/s and solubility in mol/ cm^3*Pa. A common permeability unit is Barrer.

$$1\ \text{Barrer} = 10^{10}\ \text{cm}^3\ \text{cm}\ \text{s}^{-1}\ \text{cm}^{-2}\ \text{cmHg}^{-1}$$

Hydrogen solubility in Nafion® is $2.2*10^{-10}$ mol / cm^3 Pa and is independent of the temperature, while diffusivity is depending on temperature and it is shown in the following equation:

$$D_{H2} = 0.0041 \exp(-2.602 / T) \quad (3.8)$$

Oxygen solubility is a function of temperature and it is given by the following:

$$S_{O2} = 7.43 * 10^{-10} \exp(666 / T) \quad (3.9)$$

Oxygen diffusivity in Nafion® is shown in the following equation:

$$D_{O2} = 0.0031 \exp(-2768 / T) \quad (3.10)$$

3.3 Electrodes

The electrode of a fuel cell usually consists of a thin layer catalyst between the ionomeric membrane and the porous and electrically conductive substrate. Electrochemical reactions are taking place in the surface of the catalyst. Electrons travel through electrically conductive solids, including the catalyst itself and its molecules should constantly be connected to the substrate. Protons travel through the ionomer so it should be in direct contact with the catalyst. The reactant gases travel through holes of the porous. Consequently, electrodes should always be porous and, at the same time, produced water should always be adequately removed, otherwise the electrode floods and prevents the oxygen access to the area.

The most commonly used catalyst in PEM fuel cell, for the hydrogen oxidation reaction (HOR) and the oxygen reduction reaction (ORR), is platinum(Pt). In general, catalytic surface is more important than the catalytic weight, so it is vital for the catalyst to consist of tiny parts of platinum (< 4nm) with large surface dispersed on the supported surface of the catalyst. This surface is produced from coal dust (grain size about 40nm) with a large mesoporous area and a typical support material is Vulcan XC72R.

In order to minimize the potential losses of the cell due to the rate of proton transfer and reactant gas permeation in depth of the catalytic layer, this layer should be made reasonably thin. At the same time, the active surface of the metal should be maximized and platinum particles should be as small as possible. Thus, higher Pt/C ratios should be selected, however smaller platinum particles and larger metal surfaces are achieved with a lower load. In general, higher Pt loading results in voltage gain assuming equal utilization and reasonable thickness of the catalyst layer.

The key to the optimization of the PEM fuel cell performance is the increase of platinum utilization of the catalyst layer, although it is falsely considered to be the increase of the Pt loading. The active surface of the catalyst can be enlarged by placing an ionomeric material in the catalytic layer either by painting it with solubilized PFSA in a mixture of alcohols and water or preferably by premixing catalyst an ionomer in a process of forming the catalyst layer.

Generally, there are two ways of preparing the catalytic layer and attachment to the ionomer membrane. The combination of membrane and catalyst layer is called

the Membrane Electrode Assembly (MEA). The first way of preparing the MEA is to deposit the catalytic layer on a porous substrate, which is called the diffusion layer of gas usually made of carbon fiber paper of carbon cloth and then hot-pressed into the membrane. The second way of the preparation of MEA is by applying the catalytic layers directly to the membrane, structuring the so-called tri-stromal MEA or catalytic membrane. The gas diffusion layer may be added later either as a complementary step in the preparation of MEA, or during the assembly process of the fuel cell stack.

For the deposition of the catalytic layer either in porosity substrate, or in the membrane, various ways have been developed such as:

- Spreading
- Spraying
- Sputtering
- Painting
- Screen-Printing
- Electro-deposition
- Evaporative deposition
- Impregnation

However, except for the platinum itself there are also solid metal alloys based on platinum, like PtCr, PtZr,PtTi, PtSn and PtRu which can be used as cathode catalysts[31, 35].

3.4 Gas Diffusion Layer

The layer between the catalytic layer and the bipolar disks is called a gas diffusion layer or electrode substrate or electricity collector / diffuser. Although it doesn't participate in the electrochemical reactions, it has the following functions:

- Provides the path for the reactant gasses, from the flow channels to the catalytic layer, allowing them access to the active area.
- Provides the route to the produced water, from the catalytic layer to the flow channels.
- Electrically connects the catalytic layer with the bipolar disks, allowing the electrons to close the electrical circuit.

- Conducts the heat generated by the electrochemical reactions from the catalytic layer on the bipolar disks and, finally, released to the environment.
- Provides mechanical support to the MEA, preventing it from bending and, consequently, preventing the flow in the flow channels[35].

3.4.1 Treatments and Coatings

Diffusion media are generally made hydrophobic to avoid flooding in their bulk. Both cathode and anode gas diffusion media are PTFE treated. This coating is accomplished by submerging the diffusion layer into the Teflon solution and drying it in order to evaporate the amount of water it has retained from the solution.

In addition, the interface with the adjacent catalytic layer can be covered with a coating or a microporous layer, ensuring better electrical conducts as well as efficient water transport in and out of the diffusion layer.

3.4.2 Porosity

Gas diffusion media is by definition porous. Porosity is typically between 70 ~ 80% and is easily calculated from its aerial weight, thickness and the density of the solid face. The porosity,ε, also depends on the compressed thickness:

$$\varepsilon = 1 - (W_A / \rho_{real} * d) \qquad (3.11)$$

where W_A is the aerial weight, ρ_{real} is the solid face density and d is thickness(either compressed or uncompressed)

Porosity may be measured by mercury porometry or by capillary flow porometry.

3.4.3 Electrical Conductivity

One of the functions of the gas diffusion layer is to connect electrically the catalytic layer with bipolar disks. Since only one part of the bipolar disk is in conduct with the catalytic layer (the other part is open for the gasses' access), the diffusion layer bridges the channels and redistributes electricity. For this reason, both through-plane and in-plane resistivities of gas diffusion material are important. Through-plane resistivity, ρ_Z, often includes both bulk and conduct resistance depending on the

method used in measurements. In-plane resistivity of common gas diffusion media, ρ_{xy}, typically measured by a four-point probe method is basically about an order of magnitude lower than the through-plane value.

3.4.4 Compressibility

In a fuel cell, a gas diffusion layer is compressed to minimize the contact resistance losses. Both carbon papers and carbon cloths are relatively soft and easily deformable materials. Cloth is more compressible than paper.

3.4.5 Permeability

Effective diffusion coefficients in typical PEMFC diffusion media include the effects of material porosity and tortuosity. In most cases the reflect bulk as opposed to Knudsen diffusion, since the pore diameters are several orders of magnitude higher than the mean free path of gas molecules. However, the Knudsen diffusion appeals to porous layers where the grain size can reach the mean free path of the gas molecule. Connective flow resistance of the diffusion media is given by either Gurley number or Darcy coefficient. The Gurley number is the time required to pass a specific volume of flow through a sample to a certain drop of pressure. Darcy coefficient refers to the pressure drop, which according to Darcy's law is proportional to the volumetric flow rate:

$$Q = K_D * (A / \mu * l) * \Delta P \qquad (3.12)$$

where Q is the volumetric flow rate, K_D is the Darcy coefficient, A is the cross-sectional area perpendicular to the flow, μis the gas viscosity, l is the length of the path and ΔP is the pressure drop[32].

3.5 Bipolar Plates

In a single fuel cell there are no bipolar plates. The two plates on the sides of the MEA can be considered as two parts of a bipolar disk. Bipolar disks are fully operational in a fuel cell stack connecting the anode with the cathode of the adjacent cell. Bipolar disks should have the following properties:

- Electric conductivity
- Impermeability to gases
- Mechanical strength, structural support and minimum weight
- High thermal conductivity
- Available for configuration

In addition, bipolar disks should be able to withstand the corrosion from the environment of the cell as well as not containing expensive materials to reduce the cost as much as possible[35].

One of the first materials used in bipolar disks in PEMFC was graphite, primarily because of their chemical stability. Graphite is inherently porous which can be devastating to fuel cells. Those disks should be subject to special treatment, making them impermeable to gases. This material is still being used in laboratory cells, especially in single cells. However, the cost of the treatment of the bipolar disks can be prohibitive for most fuel cell applications. Generally to categories of materials are used for bipolar disks, metal and based on graphite (including synthetic ones).

CHAPTER IV

4 COST ANALYSIS OF FUEL CELLS

Abstract

From the economic spectrum, in the current chapter, a survey concerning the costs of a PEM fuel cell system is being deducted (according to the Department Of Energy). Moreover, state-of-the-art catalysts and future challenges are mentioned.

While hydrogen fuel cells hold promise for improving the efficiency of energy consumption, especially in transportation, Pt is noticeably expensive (presently ~$1500/oz) [39], and still not an optimal electro-catalyst for ORR. A typical Pt ORR catalyst takes the form of nanometer-scale particles supported on high surface area conductive materials. Moreover, it represents about half the cost (projected by the US DOE and accounting for economies of scale) of an automotive proton-exchange membrane fuel cell (PEMFC) stack required to deliver ~80 kW [40].

Researchers' efforts in the last decades are focused on the development of cheaper electro-catalysts that outperform Pt in ORR activity, or at least achieve comparable performance at lower cost. From this perspective, activity and cost improvements have primarily been made by alloying Pt with other transition metals such as Ni, Co and Fe[41-44], whereas it has also been reported that single atomic layers of Pt can be deposited on lower cost particles, such as Pd or Au-alloys [45-49], and show improved activity.

While these multi-metallic systems outperform Pt significantly in initial activity, they also tend to be more vulnerable to deactivation than pure Pt due to dissolution of the less noble elements or of the thin Pt overlayers into the acidic PEM electrolyte[44, 50, 51]. A summary of key performance metrics for current Pt-based ORR catalyst materials and economically viable targets for automotive fuel cells (by DOE standards) is given in the *Table 1*.

Table 4.1. Current performance benchmarks and targets for Pt-based ORR catalysts for hydrogen fuel cells [38, 40, 52, 53]

Cathode Catalyst	Mass Activity	Area Activity	Durability (10% loss)	System Cost*
DOE target (Pt-based)	0.44 A/mg @0.9V	~720 μA/cm$^2_{Pt}$	5000 h	$30/kW
Commercial Pt	0.12 A/mg	200 μA/cm$^2_{Pt}$	4000 h	$75/kW
Best Pt-alloys ($Pt_{1-x}Co_x$)	0.24 A/mg	550 μA/cm$^2_{Pt}$	2500 h	$50/kW

**System costs include balance of plant expenses such as gas compressors and assembly, and advances in this area are assumed in the DOE target cost of $30/kW for a complete system.*

According to the previous table, current state-of-the-art Pt-alloy electro-catalysts can achieve about twice the ORR activity per gram of Pt-group metal (PGM), but still contribute significantly to high fuel cell stack costs as well as fall short of the DOE 5000h lifetime target (to 10% voltage loss) for most transportation applications[38, 40]. More activity enhancement will be required with better long-term stability, but necessary activity levels are likely to be even higher if mass production drives Pt prices upward.

Although no known materials can perform ORR at higher rates than Pt-based catalysts, an alternative is to focus on lower-cost catalysts. This kind of catalysts does not necessarily exhibit high activity by current standards, but is inexpensive enough

that the quantity required is unimportant. If this kind of "costless catalyst" can be utilized, activity targets can be decreased about an order of magnitude (on a catalyst volume basis) before reaching electrode thickness limits for effective mass transport and a break-even point in cost due to use of larger cell components[38, 52-54]. Performance metrics for current state-of-the-art materials, generally based on single-atom transitional-metal centers incorporated into doped graphitic frameworks, are given alongside DOE target values and Pt-volumetric activities in *Table 2*.

Table 4.2. Current performance benchmarks and targets for Pt-free ORR catalysts for hydrogen fuel cells [53, 55]

Cathode Catalyst	Volumetric Activity	Durability (10% loss)	System Cost*
DOE Target "Costless"	130 A/cm^3 @0.8V	5000h	$30/kW
Best "Costless" (nanostructured Fe-phenanthroline)	230 A/cm^3	100-1000h	$40/kW
Commercial Pt	1300 A/cm^3	4000h	$75/kW

** System costs include balance of plant expenses such as gas compressors and assembly, and advances in this area are assumed in the DOE target cost of $30/kW for a complete system.*

Finally, it is worth noting that the DOE Fuel Cell Technologies Office (FCTO) supports projects that perform and update detailed analyses to estimate cost status of fuel cell systems on an annual basis. The 2016 cost estimate of $53/kW$_{net}$ is based on Argonne National Laboratory's (ANL) projected system performance for Johnson-Matthey Fuel Cell's (JMFC) de-alloyed $PtNi_3$/C cathode catalyst (referred to as d-PtNi/C). Operating conditions and associated cost assumptions for the catalysts analyzed in 2016 are summarized in *Table 3* and are compared with cost breakdowns for the years 2011-2015[56].

Table 4.3. System design parameters and system cost evaluated at rated power from 2011 to 2016

Characteristic	Units	2011	2012	2013	2014	2015	2016
Net System Power	kW_{net}	80	80	80	80	80	80
Gross Stack Power	kW_{gross}	89.25	88.2	89.4	92.8	88.2	87.7
Stack Efficiency	%	55	55	57	55	53	52
Cell Voltage	V	0.676	0.676	0.695[a]	0.672[a]	0.661[a]	0.659[a]
Air Stoichiometric ratio		1.5[a]	1.5	1.5[a]	2	1.5[a]	1.4[a]
Stack Inlet Pressure	atm	3[a]	2.5[a]	2.5[a]	2.5[a]	2.5[a]	2.5[a]
Stack Exit Coolant Temperature	°C	90[a]	82[a]	92[a]	95[a]	94.1[a]	94[a]
Total PGM[b] Loading	mg_{PGM}/cm^2	0.186[a]	0.196[a]	0.153[a]	0.153[a]	0.142[a]	0.134[a]
MEA Areal Power Density	mW/cm^2	1100	984	692	834	746	749
Q/ΔT[c]	kW/°C	1.52	1.78	1.37[d]	1.45	1.45	1.45
System Cost	$/$kW_{net}$	49	47	55	55	53	53

a) Optimization parameter, b) PGM:platinum group metal, c) Q/ΔT is a measure of radiator size and is defined as [Stack Gross Power(1.25V-Cell Voltage at Rated Power)/(Cell Voltage at Rated Power)]/ [(Stack Coolant Exit Temperature(°C)- ambient temperature(40 °C)], d) In 2013, the heat of condensation was accounted for in the Q/ΔT calculation resulting in an operating point satisfying Q/ΔT with a higher cell voltage than would be calculated using the definition in footnote b above.*

In addition, the Strategic Analysis, Inc. (SA) cost analysis is based on beginning of life performance of membrane electrode assemblies (MEA) made with the JMFC d-PtNi/C cathode catalyst and a Pt/C anode catalyst on 17 micron reinforced Nafion® membranes. As in past analyses, the Pt commodity price was fixed at $1500 per troy ounce to remove Pt price fluctuations from the analysis that could otherwise obscure improvements due to technology advancements. This cost estimate is based on materials price quotes obtained between 2012 and 2016. All calculations were performed using nominal year dollars.The results of 2016 cost analysis are graphically compared with prior year results in *Figure 1*. There is no net change in projected system cost at 500000 units per year between 2015 and 2016.

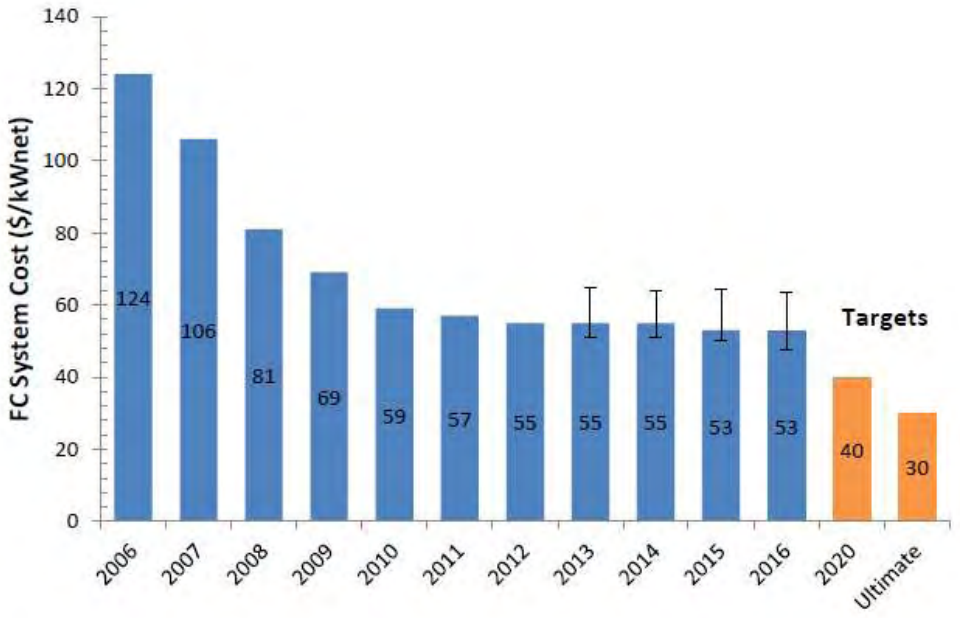

Figure 4.1. Modeled cost of an 80-kWnet PEM fuel cell system based on projection to high-volume manufacturing (500000 units/year)[57]

Moreover, the SA analysis indicates that the fuel cell stack would account for 71% and 52% of the total system cost at 1000 and 500000 systems per year, respectively. A breakdown of stack component cost is shown in *Figure 2*. Among the various components, two (catalyst and bipolar plates) are dominated by commodity materials costs (platinum and stainless steel, respectively), which are relatively insensitive to manufacturing volume. The rest of the component costs are dominated by specialty materials and processing costs, which are more sensitive to volume. Thus, an increase in production volume causes the membrane and gas diffusion layer

(GDL) cost elements to decrease as a fraction of the total, while the catalyst and bipolar plate cost elements increase.

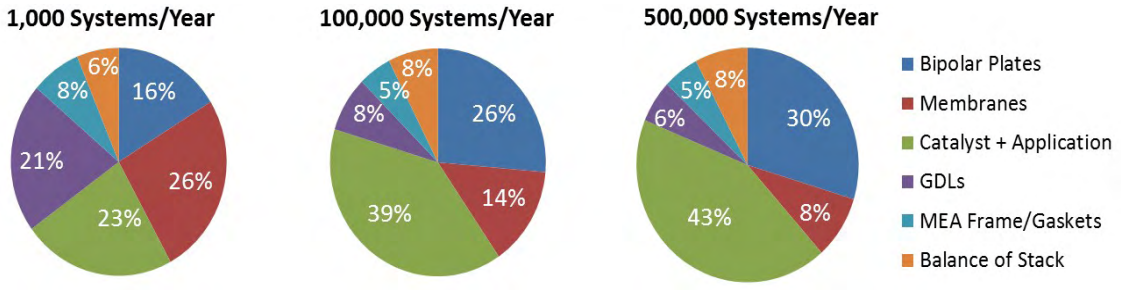

Figure 4.2. Breakdown of the 2016 projected fuel cell stack cost at 1000, 100000 and 500000 systems per year

The expected cost of a 90 kW_{net} automotive PEM fuel cell system based on technology currently ready for commercialization is approximately $230/kW when manufactured at a volume of 1000 units/year[58].This cost estimate is based on the inputs of several auto-manufacturers and on resources that describe the design of commercially available light-duty vehicles. The difference in projected cost of a commercially available fuel cell system ($230/kW at 1000 systems/year) and the reported 2016 status system ($197/$kW_{net}$ when the analysis is extrapolated to a comparable 90kW_{net} system at 1000 units/year) is that the 2016 status system is based on next generation lab-demonstrated components while commercially available systems prioritize durability and near-term robustness over cost. Thus, the commercially available technology design uses coated titanium plates rather than coated stainless steel plates, higher catalyst loading (0.3 vs 0.134 mgPt/cm^2), and manufacturing methods appropriate for early market introduction.

In contrast, the 2016 status system assumes the use of design and fabrication methods based on the state-of-the-art technologies, largely demonstrated in the lab or with modeling, but not yet proven in a relevant manufacturing environment. Additionally, the 2016 status system is designed to achieve initial system performance and may not have the same levels of durability as the commercially available system.

CHAPTER V

5 HYDROGEN OXIDATION AND OXYGEN REDUCTION REACTIONS OVER Pd_XIr_Y ELECTROCATALYSTS FOR PEMFC APPLICATIONS

Abstract

Finally, in chapter 5, preparation and examination of the catalysts are thoroughly presented. Experimental analysis is extensively reviewed step by step. Specific results are being demonstrated and compared aiming to contribute to the already existing literature.

5.1 Introduction

Through the last decades, governments have begun to seriously consider the hydrogen options. Hydrogen is an attractive energy carrier and storage medium, with high efficiency for developing a low-emission, environmentally friendly, clean and sustainable energy system in order to help solve the world's energy security and environmental problems[59]. However, numerous technical infrastructure challenges in the area of production, distribution, storage and end use must be resolved for hydrogen to have an important role in earth's energy and environment's future[60].Generally, fuel cells directly covert the chemical energy of H_2 to electricity. However, the commercialization of this device (for example PEMFC) is still hindered because of its high cost. The platinum-based catalyst is mainly

responsible for the cost and a characteristic range of costs of the catalysts is shown at the following diagram.

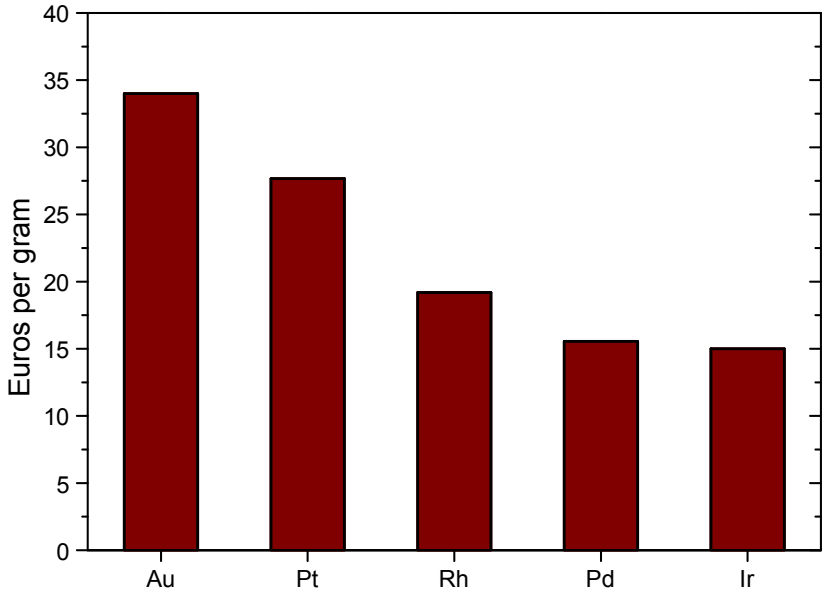

Figure 5.1. Average price of noble metals for the first semester of 2016 [61]

Therefore, in order to improve the catalytic activity, reduce the cost and increase the durability of the catalysts, many attempts have been made to design novel Pt-based and Pt-free electrocatalysts for hydrogen oxidation reaction (HOR) and oxygen reduction reaction (ORR). With the exception of Pt, the electrocatalytic activity of Pd is one of the highest among the pure metals for both HOR and ORR. This, combined with the fact that Pd cost is about half the cost of Pt, makes it an attractive alternative[61].

Research has shown that in acidic environment Pd-based electrocatalysts exhibit better activity than those based on Pt due to high solubility, permeability and selectivity for hydrogen[62-64].In order to enhance the HOR activity of pure Pd various Pd-based catalysts with novel nanostructures (hollow, porous, core/shell, near-surface alloys, etc.) have been synthesized[65, 66].Some distinct examples are bimetallic Pt-Pd[67, 68], Pd-Ru[69], Pd-Ni[70] and trimetallic Pd-Pt-Rh[71], Pd-Ru-WO_x[72].

One of the most extensively studied subjects in fuel cell research is the performance of the catalyst used for the oxygen reduction reaction. Moreover, researches have proven that Pd bimetallic nanostructures are the most interesting cathode materials because of their superior catalytic activity[73, 74]. During the

studies, it has been found that the catalytic activity and stability of Pd-based alloys for the ORR is enhanced by the addition of other elements, which could modify its electronic structure into core-shell type catalyst [75, 76]. Bimetallic combinations such as Pd-Ni [77], Pd-Co [78, 79], Pd-Cu [80-83], Pd-Fe[84, 85] have demonstrated to be the most active catalysts because of their moderate interaction with oxygen in acidic media[74]. Furthermore, iridium is another metal which belongs to the platinum group (Figure1) and according to theory [86] it should exhibit almost similar activity as platinum toward HOR and ORR. However, very few recorded studies in literature have been devoted to Pd-Ir bimetallic electrocatalysts for HOR and ORR [87-91].

The catalytic activity of several Vulcan XC-72 supported Pd, Ir and Pd_xIr_x (where x: y= 3:1, 1:1, 1:3) electrocatalysts was separately tested in the present work for the reactions of hydrogen oxidation and oxygen reduction. The examined electrocatalysts were prepared by a modified pulse-microwave assisted polyol synthesis method. Their corresponding physic-chemical characteristics were obtained by using transmission electron microscopy (TEM) and X-ray diffraction (XRD), while their electrocatalytic activity toward the reactions of hydrogen oxidation and oxygen reduction was measured in acidic environment by cyclic voltammetry (CV) and rotating disk electrode (RDE) techniques.

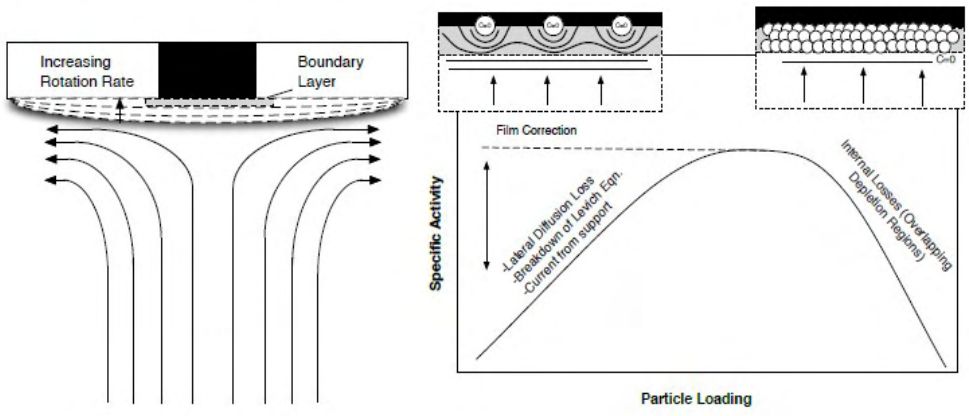

Figure 5.2. Rotating disk electrode operating principle and behavior with catalyst particle active layers

**Left:Schematic of RDE apparatus and flow pattern. Right: Qualitative relationship between measured specific-activity of catalyst particle layer and catalyst loading on an RDE.*

5.2 Experimental

5.2.1 Electrocatalysts preparation

The 20 wt % Pd_xIr_x supported on Vulcan-XC 72 carbon catalysts were prepared via a modified pulse-microwave assisted polyol synthesis procedure[92]. The primary steps of the synthesis process were: the starting precursors ($PdCl_2 2H_2O$ and $IrCl_2$ provided by (Strem Chemicals) were added in a beaker with ethylene glycol (EG) and were well mixed in an ultrasonic bath. Then, Vulcan XC-72 carbon black (Cabot Corporation) was added into the above mixture. Consequently, the pH value of the system was adjusted to 13 by the drop-wise addition of 1.0 M NaOH/EG and a well-dispensed slurry was obtained with ultrasonic stirring for 60 min. Thereafter, the slurry was microwave-heated in the pulse form 10s on/ 10s off, for several times. In order to promote the adsorption of the suspended metal nanoparticles onto the carbon support, hydrochloric acid was adopted as the sedimentation promoter and the solution was re-acidified with a pH value of about 2-4. The obtained black solid sample was filtered, washed and dried at 80° C for 10 hrs in a vacuum oven[93]. Similar procedures were followed for the preparation of 20 wt % Pd/Vulcan XC-72 and 20 wt % Ir/Vulcan XC-72.

5.2.2 Physicochemical Characterization

Catalysts were investigated by TEM using Philips CM12 microscope (resolution 0.2nm), provided with high resolution camera, at an accelerating voltage of 120 kV. Suitable samples for TEM analyses were prepared by ultrasonic dispersion in i-propylic alcohol adding a drop of the resultant suspension onto o holey carbon supported grid. The X-ray diffraction (XRD) measurements were achieved with the help of a D/Max-IIIA (Rigaku Co., Japan) employing CuKa (λ = 0.15406 nm) as the radiation source at 40 kV and 40 mA.

5.2.3 Electrochemical characterization

Electrochemical measurements were carried out with the assistance of AMEL 7050, in a three-electrode model cell 497 (AMEL) with a mercury/mercury oxide

($Hg/HgCl_2$) (0.098 V vs SCE) and platinum wire as the reference electrode and counter electrode, respectively.

The catalytic ink was prepared by dispersing 5.0 mg of the as-prepared powder (electrocatalyst), 1.8 mL ethanol and 0.2 mL Nafion solution (5 wt %, Dupont Company). The suspension was ultrasonicated for 40 min to obtain a well-dispersed ink. Then 6μL of the as-prepared ink was transferred onto the working electrode, where was dried with the aid of an infrared lamp.

All the electrochemical measurements were conducted in 0.5 mol L^{-1} H_2SO_4 (Carlo Erba, 96%) aqueous solution, at 25°C.Before each experiment, the solution was bubbled for 30 min with high-purity N_2 in order to remove the dissolved oxygen. Moreover, before each measurement, each catalyst was applied under continuous potential cycling until stable electrochemical signals were received.

5.3 Results and Discussion

5.3.1 Physicochemical characterization

In *Fig. 5.3* the XRD patterns of the as prepared Pd, Ir and Pd_xIr_y catalysts are schematically shown. Except for the characteristic peak of Vulcan XC-72 at 24.5°,also 2θ values of four more peaks at 40.07°, 46.53°, 68.19◦ and 82.02°, that correspond to face-centered cubic (fcc) crystalline Pd(1 1 0), (1 1 1), (2 0 0), (2 2 0) and (3 1 1), appear respectively. The highest intensity of peak from (1 1 1) plane indicates that this is the most exposed face of the Pd_xIr_y/C nanoparticles. The peak position of (1 1 1) plane of Pd_xIr_y/C electrocatalysts is between the Pd/C's and Ir/C's peaks position.In addition, no characteristic peaks related to Ir were observed, further supporting that a Pd-Ir alloy has been formed via insertion of Ir into Pd lattice. For example, the 2θ values of the four peaks of Ir and $PdIr_3$ catalysts are 40.06°, 46.91°, 67.89° and 84.09°, respectively (*Fig. 3*curve e and d) and they are 39.04°, 45.51°, 66.55° and 82.00°, respectively, for the PdIr and Pd_3Ircatalyst (*Fig. 5.2*, curve c,b)[94].*Table 1* lists the crystallite sizes and the corresponding lattice parameters calculated using the Scherrer formula and Bragg equations, respectively[95].All the examined catalysts have crystallite sizes ranged between~3.5-4.0nm.

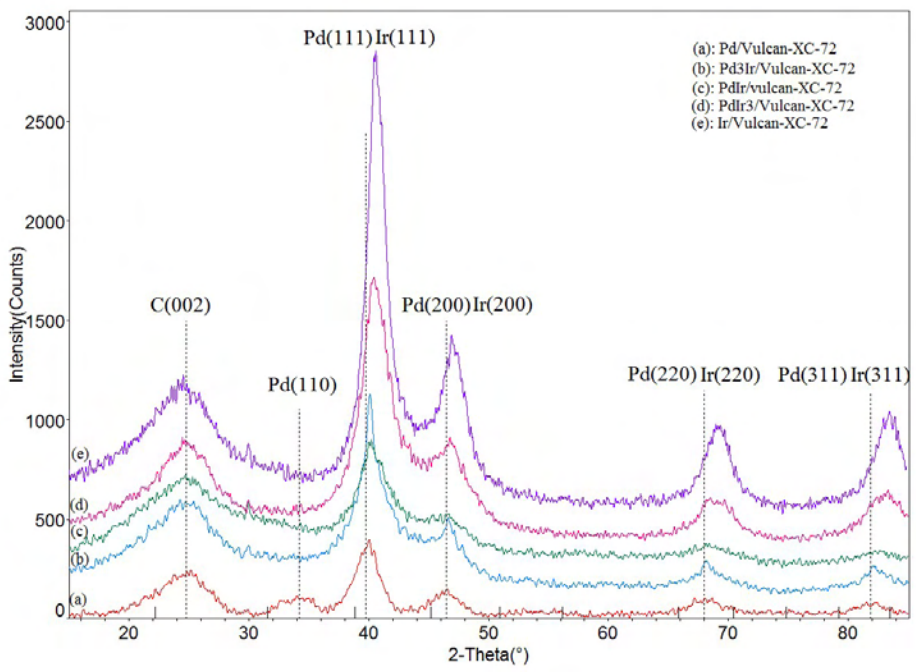

Figure 5.3. XRD patterns of Vulcan XC-72 supported: (a) Pd, (b) Pd3Ir, (c) PdIr, (d) PdIr3 and (e) Ir

Table 5.1. Results obtained from the physicochemical characterization

Electrocatalyst	Lattice Parameter (nm)	Crystallite Size (nm)	Internal distance (nm)	Particles Size (±0.3nm)
Pd	0.38615	3.00	0.18701	4.30
Ir	0.38448	3.50	0.16655	5.70
Pd_3Ir	0.38843	3.50	0.16835	4.50
PdIr	0.38810	3.00	0.16812	4.40
$PdIr_3$	0.38503	4.00	0.16688	5.30

The mean size of the nanoparticles and their structure were further evaluated by the aid of TEM. The TEM micrographs with the respective particle size distribution histogram of the examined electrocatalysts are depicted in *Fig. 5.4.* It can be observed that, for Pd, Pd_3Ir and PdIr the metallic nanoparticles are homogenously dispersed on the carbon support with narrow size distribution in the supported catalyst. Ir and $PdIr_3$ have non-spherical morphologies and some larger aggregates were observed, but the amount of

particles is few. One hundred particles were randomly measured to obtain the particle size distribution.The average particle sizes of the prepared catalysts are reported in *Table 5.1*.

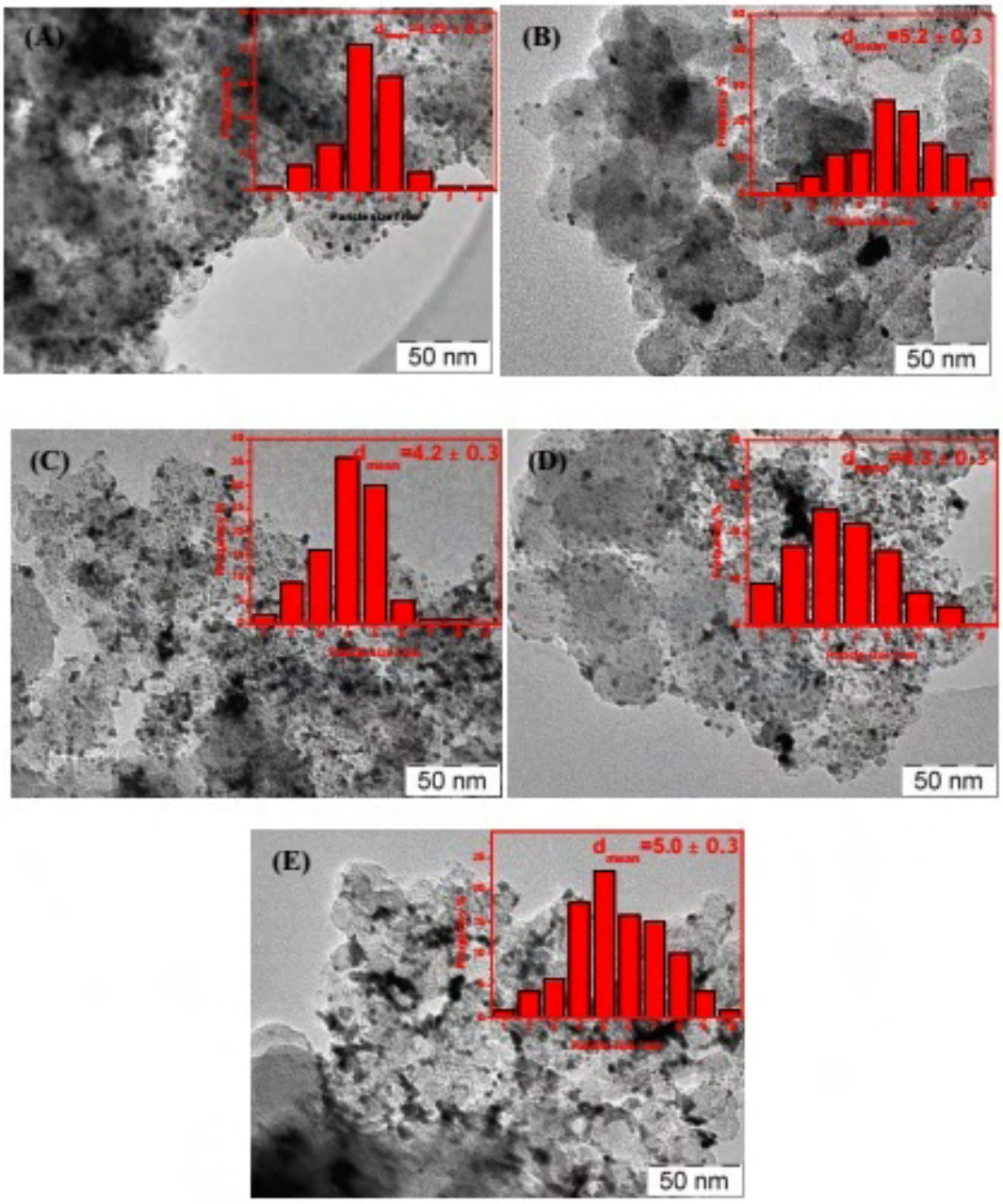

Figure 5.4. TEM images and corresponding of (A) Pd/ Vulcan XC-72, (B) Ir/Vulcan XC-72, (C) Pd3Ir/Vulcan XC-72, (D) PdIr/Vulcan XC-72, (E) PdIr3/Vulcan XC-72

5.3.2 Electrochemical characterization

5.3.2.1 Cyclic voltammetry – Electrochemical active surface area

For the estimation of the electrochemical active surface areas the technique of cyclic voltammetry was used as presented in *Fig. 5.5*. The electrochemical active surface area is the real surface area of the catalyst which determines the catalytic activity.

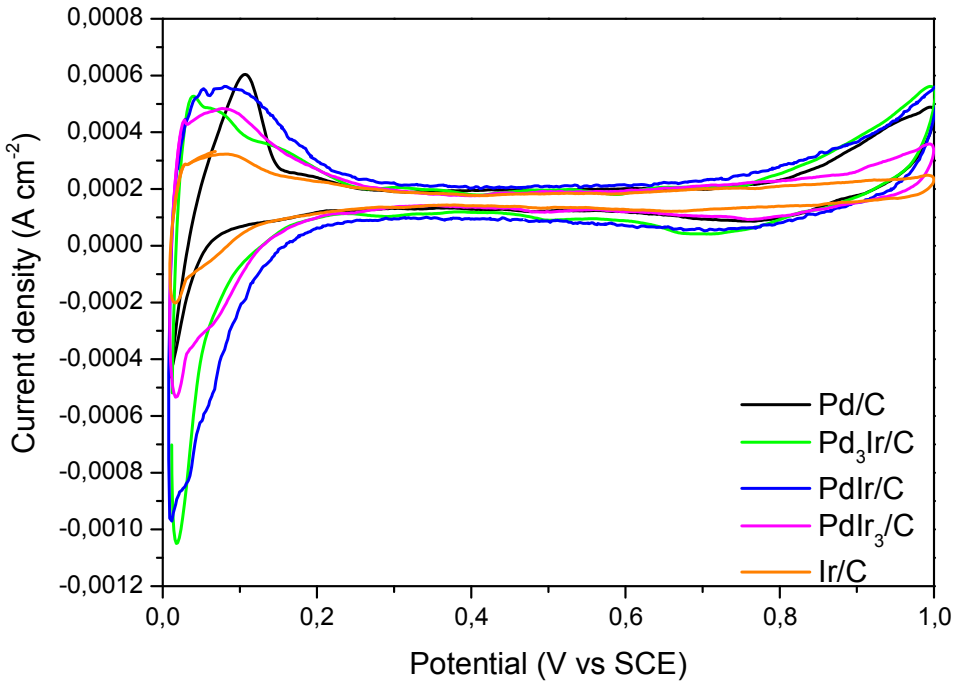

Figure 5.5. Cyclic voltammagrams in oxygen saturated 0.5M H¬2SO4 electrolyte at 25oC and at a scan rate of 20 mVs^{-1}

From the voltammetric features(*Fig.5*), adsorption and desorption of hydrogen appears within the potential range of 0.0 to 0.3 V, the double layer capacitance region is from 0.3 to 0.6 V and the formation of oxides at potential more positives than 0.6 V. Furthermore, the onset of the reduction of the surface oxide in the cathodic scan is observed at ca 0.7 V vs SCE.

The electrochemical active surface area, taking into consideration the cyclic voltammograms and the following mathematical equation, is calculated by:

$$ECSA\left[\frac{m^2}{g}\right] = \frac{Q_H}{Q_{(monolayer)} \times m_{Pd\ or\ Ir} \times 10} \qquad (5.1)$$

where Q_H ($\mu C cm^{-2}_{Pd}$) is the integrated surface of the hydrogen adsorption peak, $Q_{Pd\ or\ Ir}$(=210μCcm$^{-2}_{Pd}$)[96, 97] are the specific amount of electricity corresponding to the full coverage of the Pd or Ir surface by one monolayer of oxygen (μCcm^{-2}) and $m_{Pd(Ir)}$ ($mg cm^{-2}_{electrode}$) is the palladium or iridium loading on the working electrode's surface.

The estimated ECSA are reported in *Table 5.2*. Among the examined electrocatalysts PdIr has significant higher ECSA, 270 m^2g^{-1}, followed in sequence, by the Pd_3Ir, $PdIr_3$, Pd and Ir.

Table 5.2. Estimated electrochemical active surface areas

Electrocatalyst (supported on Vulcan XC-72)	**ECSA $(m^2\ g^{-1})_{Pd\ or\ Ir}$**
Pd	50.00
Pd_3Ir	131.0
PdIr	270.0
$PdIr_3$	113.0
Ir	39.50

5.3.3 Hydrogen oxidation reaction

Hydrogen oxidation reaction (HOR) has been thoroughly investigated on Pt surfaces[98]. Three fundamental reaction steps are included for HOR on a Pt surface, based on the Tafel–Heyrovsky–Volmer mechanism[99]:

Tafel Equation: $H_2 \rightleftarrows H_{ad} + H_{ab}$ (5.2)

Heyrovsky reaction: $H_2 \rightleftarrows H_{ad} + H^+ + e^-$ (5.3)

Volmer reaction: $H_{ad} \rightleftarrows H^+ + e^-$ (5.4)

The most renown mechanism for the hydrogen oxidation reaction (HOR) on polycrystalline metals in acidic media consists of two steps: the first step, which involves the adsorption of molecular hydrogen on a surface active metal site either by the dissociation of hydrogen molecules into adsorbed atoms (Tafel process) or by the dissociation into ion and adsorbed atom (Heyrovsky process) and the second step, which includes charge transfer procedure (Volmer process)[100].

Since the electronic properties of Pd are very similar to those of Pt, the HOR on Pd surfaces should follow the same pathways proposed for Pt[75].The HOR polarization curves are depicted in *Fig.5*. As it can be observed, the oxidation of H_2 over the Pd_xIr_y/C alloys and pure Ir/C starts at potential values around to 0.01 V (onset potential), while over pure Pd/C electrocatalyst the HOR's onset potential is higher, ca 0.1 V. At more positive potentials, transition into the region of hydrogen mass transport controlled current densities starts at approximately 0.15 V for the PdIr/C, $PdIr_3$/C and Ir/C, while for the Pd/C and Pd_3Ir/C starts at 0.2V.As it was expected, the limiting current increases with the increment of the rotational speed of the electrode[101].

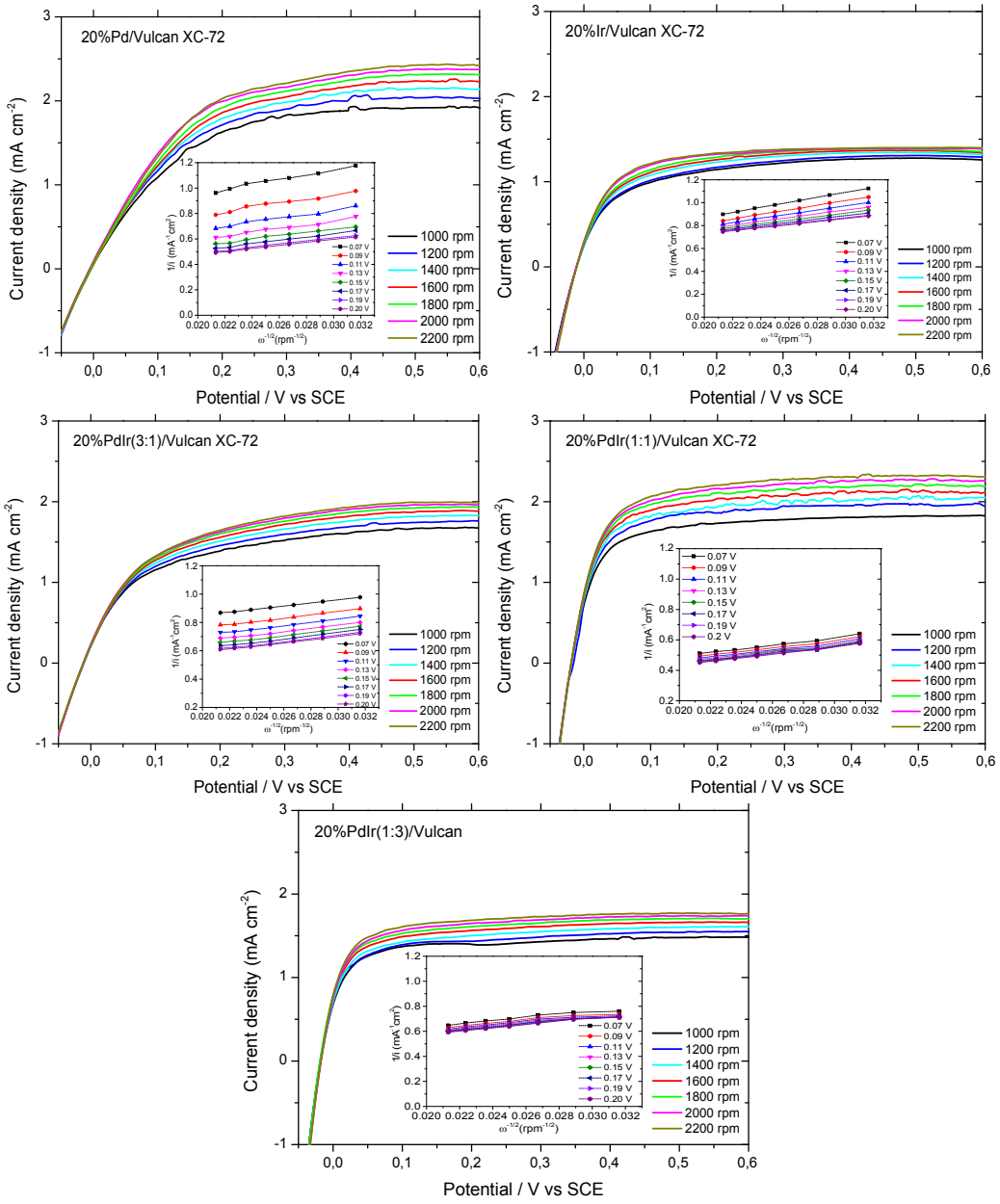

Figure 5.6. RDE curves in H2-saturated 0.5 M H2SO4aqueous solution at 5 mVs-1. The insets are the corresponding Koutecky-Levich plots for the hydrogen oxidation reaction.

As it is known, kinetic current density (i_k)is a measure of the rate of charge transfer on the catalyst's surface, describing the real kinetics of an electrocatalytic reaction and, therefore, is directly related to the electrocatalyst's activity. To determine the catalytic activity of the electrocatalysts, the Koutecky–Levich[102, 103] analysis[104, 105]has been adopted, where the kinetic current is related to the rotational velocity of the RDE through the following equation:

$$\frac{1}{i}=\frac{1}{i_k}+\frac{1}{i_d} \tag{5.5}$$

In *Equation 5.5* i is the measured current density, i_k the kinetic current in absence of mass transfer limitations and i_d the diffusion current density. The later (i_d) can be calculated according to the Levich equation:

$$i_d = 0.62nFD^{2/3}v^{-1/6}C\omega^{1/2} \tag{5.6}$$

where n represents the number of theoretically-transferred electrons (=2), F the Faraday constant (95485 C/mol), D the diffusion coefficient of H_2 in H_2SO_4 (3.7×10^{-5} cm^2 s^{-1}), v the kinematic viscosity of the electrolyte and C the H_2 concentration in the electrolyte (7.14×10^{-7} mol cm^{-3}).

In the insets of *Fig.6* the respective Koutecky-Levich plots are depicted at different potential values. According to the plots, the kinetic currents for HOR, at different potential values (vs SCE), were extracted. Further analysis proves that the experimental points exhibit a linear behavior ensuring the accuracy of n and i_k determination. In *Table 3* the calculated kinetic current density values at 0.07V are documented. Moreover, for 1:1Pd:Ir ratio, the highest kinetic current density is exhibited, while for 3:1, the lowest one.

Table 5.3. Kinetic parameters of the examined electrocatalysts for HOR

Electrode (20%wt metal loading)	**Tafel slope (mV decade^{-1})**	i_o **(mA cm^{-2})**	$i_k\,(@\,0.07\ V)$ **(mA cm^{-2})**
Pd/ Vulcan XC-72	80.0	0.35	2.50
Pd_3Ir/Vulcan XC-72	95.0	0.70	2.80
PdIr/ Vulcan XC-72	120	1.60	4.70
$PdIr_3$/ Vulcan XC-72	50.0	1.00	3.50
Ir/ Vulcan XC-72	71.0	0.20	1.40

Additionally, from Tafel equation's analysis useful kinetic information to measure the electrochemical activity of an electrode material can be obtained[106]. Exchange current density is analogous to the rate constant used in chemical kinetics, and a high i_o value often translates into a fast electrochemical reaction:

$$\log(i_k) = \log(i_o) + (\frac{anF}{2.303RT})\eta \quad (5.7)$$

On the other hand, from the kinetic analysis point of view a smaller Tafel slope is preferable (for smaller overpotential values). Moreover, according to literature[98], the slope values and the hydrogen oxidation reaction are well described by the Tafel–Heyrovsky–Volmer mechanism.

In *Fig. 7*, as the Tafel plots show, it is obvious that, among the investigated samples, PdIr/C exhibits the highest electrocatalytic activity towards hydrogen electro-oxidation. Furthermore, according to the theoretical estimation and the calculated Tafel slopes (around and higher than 60 mVdecade^{-1}, *Table 3*),the results are well described by the Tafel-Volmer mechanism *Eqs (2) & (3) & (4)*, with the Volmer to play the role of the rate determining step[107]).

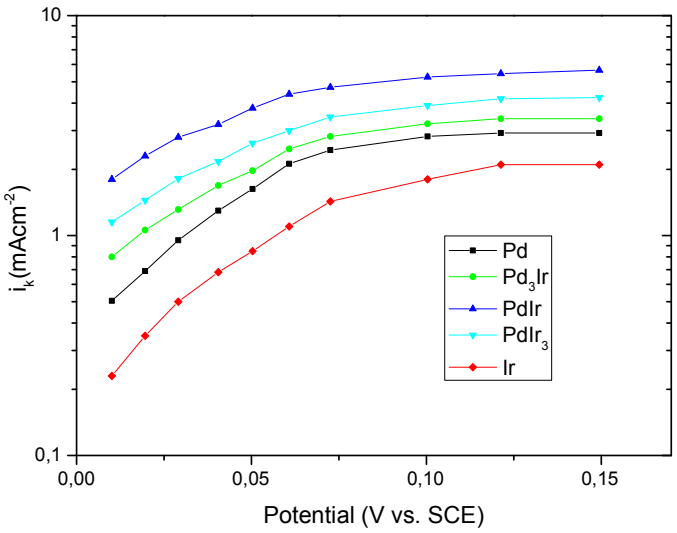

Figure 5.7. Tafel plots for HOR

The effect of Ir loading to Pd on the HOR electro-catalytic activity is schematically given in *Fig. 8*. The increase of Ir loading enhances the electrocatalytic activity of Pd reaching a maximum for 50:50 (Pd:Ir) atomic ratio, with kinetic current

density of 4.7 mA cm^{-2}, respectively

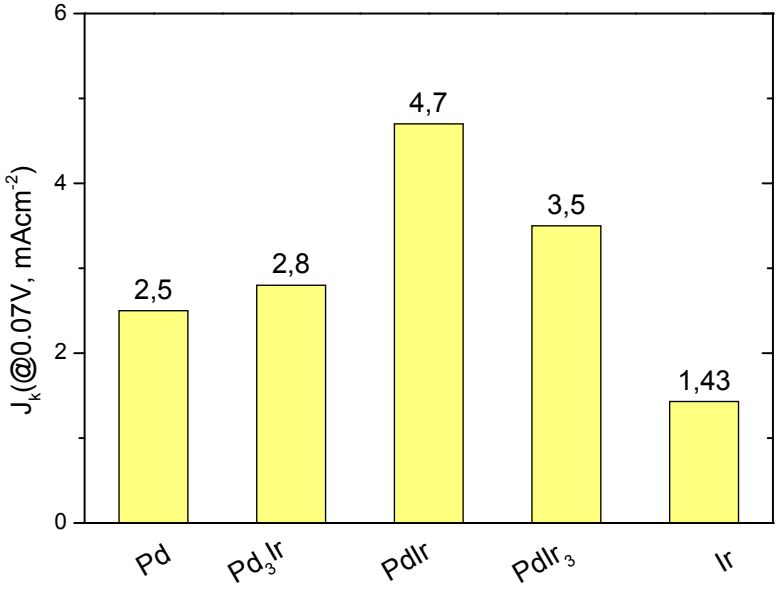

Figure 5.8. Kinetic current density vs iridium metal loading for HOR

The reaction of hydrogen electro-oxidation over bimetallic palladium-iridium electrocatalysts is affected by the Pd/Ir ratio, as it is described in literature[108]. More precisely, HOR catalytic activity of the Pd_xIr_y alloy catalysts is correlated to iridium's d-band vacancy exhibiting volcano type dependence between kinetic current density and Pd percentage as well as between the kinetic current density and d-band vacancy. This behavior is attributed to the fact that HOR activity is given by the strength of the Ir-H bond interaction, which depends on the position of the Ir d-band states relevant to the Fermi level. The "extent" of d-band vacancy could affect the "extent" of the electrocatalytic activity of the prepared electrode materials. The same volcano behavior is observed also in the current study *(Fig.8)*.

5.3.4 Oxygen reduction reaction kinetics

The ORR activity of the prepared electrocatalystswas investigated in aqueous O_2-saturated 0.5 M H_2SO_4 solution under different rotation rates (from 800 to 1800rpm) at a scan rate of 10 mV s^{-1}.As it can be seen from *Figure 9*, the ORR curves can be distinguished in three typical regions: i) the kinetic (0.6–0.8 V), ii) the mix-controlled (0.2–0.6 V) and iii) the diffusion (0.0–0.2 V).

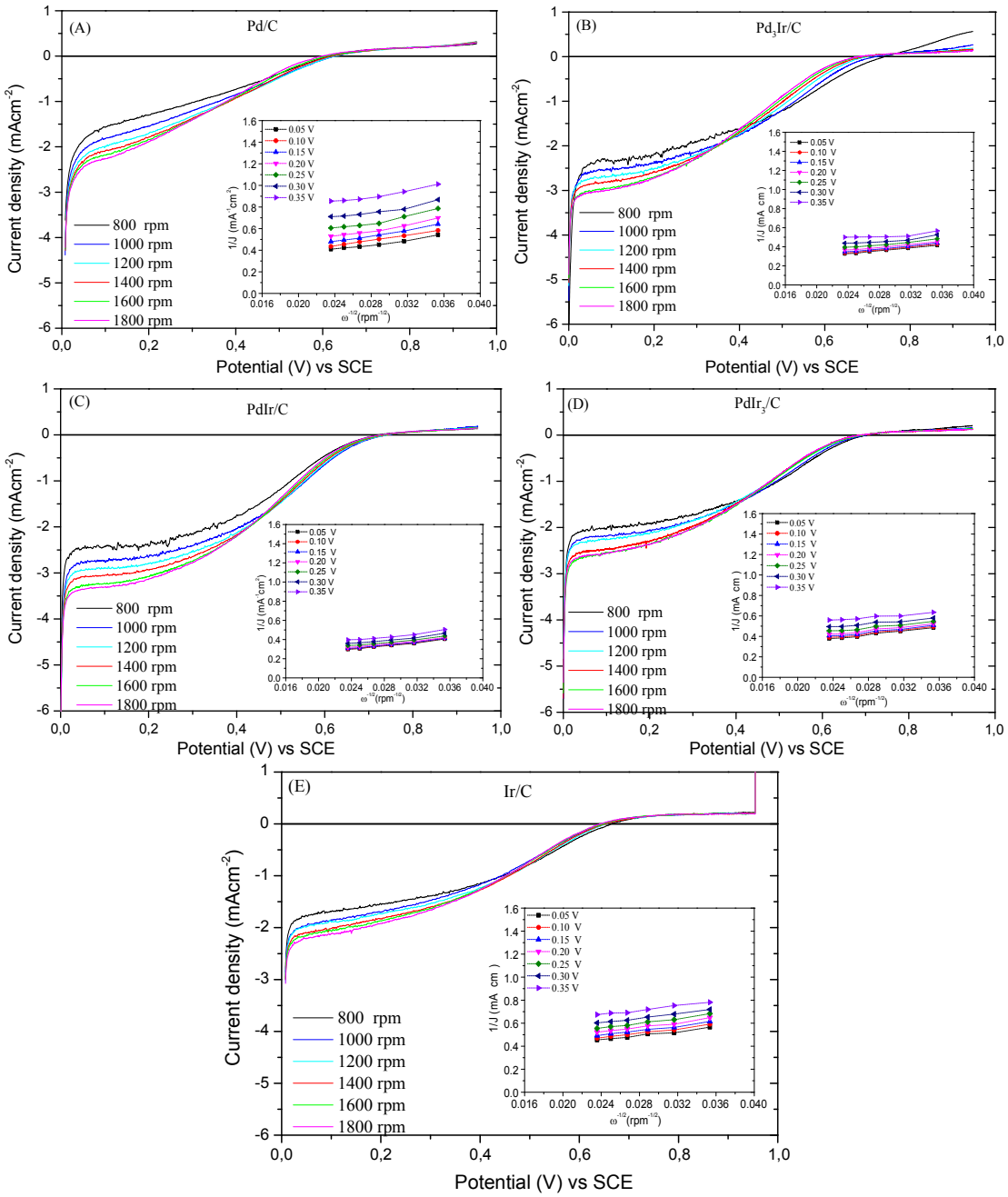

Figure 5.9. Potential curves for ORR of the examined electrocatalysts at different rotation rates, in 0.5 M H2SO4 aqueous solution. Inset: Koutecky–Levitch plots at various electrode potentials from 0.05 to 0.35 V

In the potential range of 0.0–0.2 V, the currents depend on the rotation rate and display well-defined limiting currents (plateau), indicating that the currents are controlled by the rate of O_2 diffusion from the solution's bulk to the catalyst-electrode surface. In the potential range between 0.7 and 0.2 V, both molecular oxygen mass transfer (diffusion) and electron transfer kinetics contribute to the current.

The kinetic parameters, kinetic current density and the number of electrons transferred during the reaction, can be analyzed on the basis of the Koutecky–Levich equation *(Eqs 5 & 6)* and Koutecky-Levich plots (insets of *Fig 5.9*). Concerning the calculations, the values of F (= Faradaic constant, 96486.7 $Cmol^{-1}$), C_o(bulk concentration of oxygen)=$1.13x10^{-3}$M, D (diffusion coefficient for oxygen)=$1.8x10^{-5}cm^2s^{-1}$ and ν (viscosity of electrolyte)=$10.78x10^{-2}$ cm^{-2}[109]were used.

The ORR is a multi-electron reaction, consisting of elementary steps and different reaction intermediates. During ORR, two main reactions usually occur on the catalyst surface, as it is described with equations (1) and (2):

$$O_2 + 2H^+ + 2e \rightarrow H_2O_2 \quad (1)$$

$$H_2O_2 + 2H^+ + 2e \rightarrow 2H_2O \quad (2)$$

Hydrogen peroxide is the intermediate species when ORR proceeds via the two-electron pathway[110]. From the kinetic analysis, the electron transfer number for pure Pd/C and Ir/C electrocatalysts is one, while for bimetallic Pd_xIr_y/C is two. This result indicates that hydrogen peroxide could be the main product. The direct ORR pathway via a 4-electron transfer is desirable rather than the 2-electron transfer pathway, which may negatively affect the stability of the catalysts[111].

Tafel plots were extracted from the kinetic current density values as shown in *Figure 5.10*. Two regions with distinct slope values are observed as it is reported in *Table 5.4.* In the low overpotential region, the slope was close to 60 mV dec^{-1}, while at high overpotential region was close to 120 mV dec^{-1}. This difference may indicate a possible change of reaction mechanism or change of the rate-determining step[112]. For example, a Tafel slope value of 120 mV indicates that the first electron transfer should be the rate-determining step: $O_2 + e^- \rightleftarrows O_{2,ads}$[113].

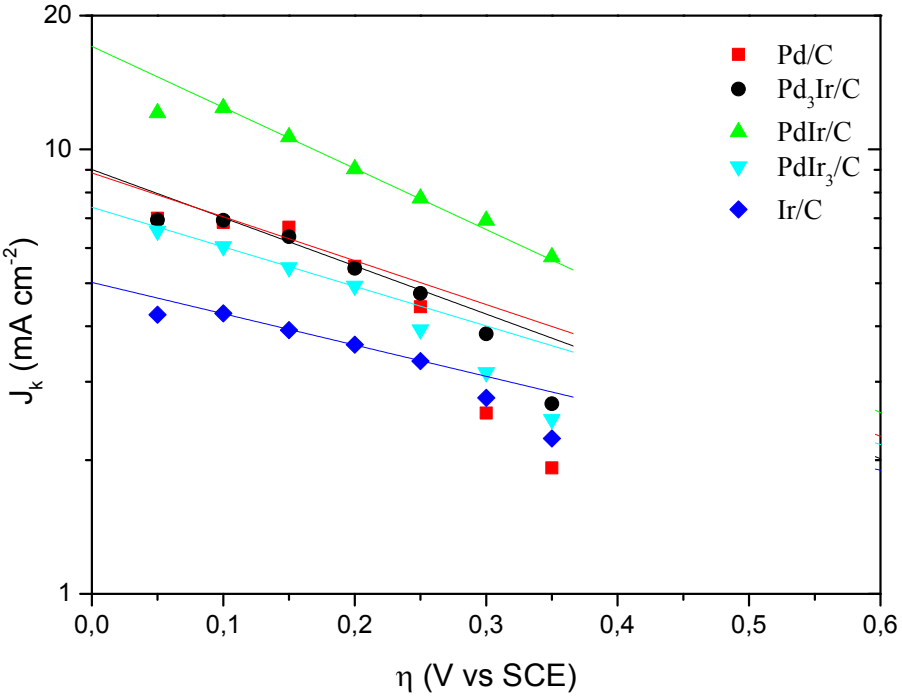

Figure 5.10. Tafel plots for the ORR

In general, Ir possesses a promoting action in alloys as it is has also been stated by Birss, V.I *et al* [114].In order to better realize the effect of Ir loading on catalytic activity of pure Pd, *Figure 5.11* is shown. A volcano behavior of kinetic activity is observed according to the calculated kinetic current density values. Comparing with HOR results, concerning ORR, the maximum kinetic current density (5.7 mA cm^{-2}) counts when the atomic ratio Pd:Ir is 50:50. Further Ir's addition suppresses by ~57% electrocatalyst's catalytic activity (2.46 mA cm^{-2}).

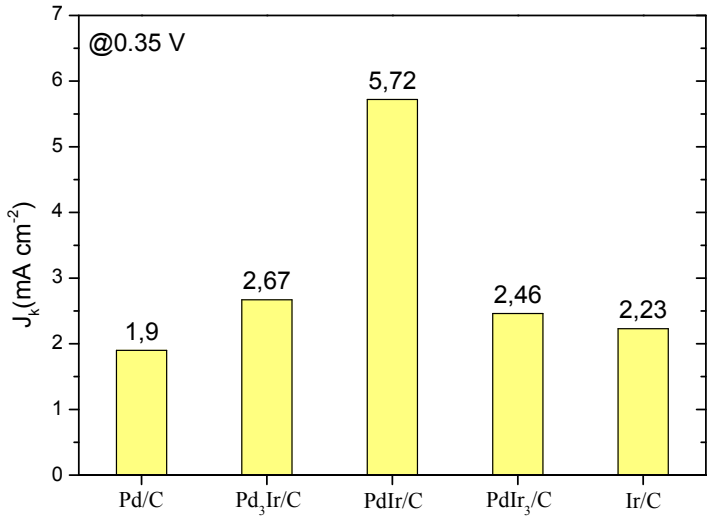

Figure 5.11. Kinetic current density vs iridium metal loading for ORR

Table 5.4. Kinetic parameters extracted from Tafel analysis for the ORR

Electrode	Tafel slope at low overpotential (mV dec^{-1})	Tafel slope at high overpotential(mV dec^{-1})
Pd/Vulcan XC-72	27	84
Pd_3Ir/Vulcan XC-72	52	90
PdIr/Vulcan XC-72	60	90
$PdIr_3$/ Vulcan XC-72	50	112
Ir/ Vulcan XC-72	57	141

The addition of Ir to Pd, positively affects the values of kinetic current density, exhibiting a volcano-type dependence on the Pd:Ir atomic ratio. As in similar cases reported in literature[89], the observed volcano behavior could partly be attributed to electronic reasons. More specifically, the addition of Ir to Pd increase the extent of Pd's d-vacancy, increasing the oxygen π electrons donation to the surface of Pd, enhancing consequently oxygen adsorption and weakening of the O-O bonds. Another reason could also be attributed to the fact that Ir atoms exposed to the catalyst surface

are likely to be covered by OH_{ads} at more negative potentials than Pd, because the onset potential of the OH_{ads} region for Ir is more negative than that for Pd. Thus, the Ir atoms could predominantly be covered by OH_{ads} at the first stage of the OH_{ads} formation, leaving more Pd sites free for the ORR, which may partly lead to the enhanced kinetics of the Pd-Ir alloys[89].

Therefore, according to the generally accepted four-electron transfer mechanism of oxygen reduction it seems that the O-O bond breaking and the O-H bond formation are not favored with Pd_xIr_y/C electrocatalysts. It seems that this loading of Ir is not enough for binding the oxygen strongly and the OH modestly, so that OH removal from the catalyst surface by water elimination to be also reasonably facile.

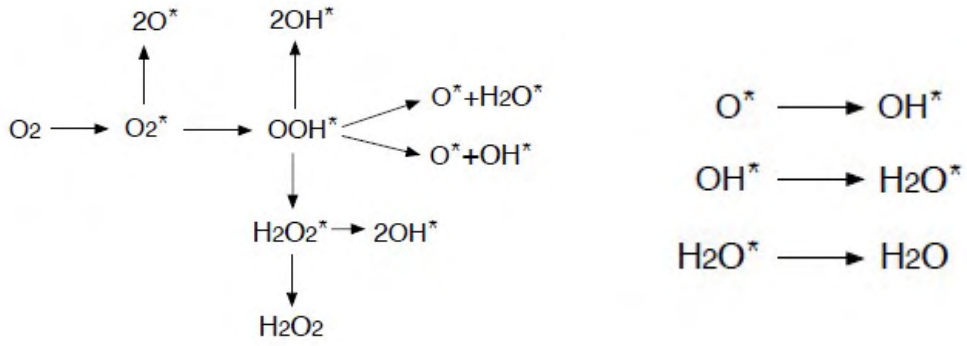

Figure 5.12. Possible ORR reaction pathways

5.4 Conclusions

In the present work, Vulcan XC-72 carbon supported Pd_xIr_y, Pd and Ir catalysts with relatively high nanoparticles dispersion were successfully synthesized by the aid of a pulse-microwave assisted polyol method. Based on the experimental results, it could be concluded that the use of the above synthesis method is an effective way to get carbon supported electrocatalysts with high dispersion in a short time and with low cost. According to the electrochemical results obtained, it seems that in all cases the addition of Ir enhances the electrocatalytic activity of Pd toward hydrogen oxidation and oxygen reduction reaction. In both cases a volcano-type current density dependence on Ir-loading is observed. The lower values have been

observed for pure iridium and pure palladium. From the Koutecky–Levich plots, the ORR the electron transfer number ~2 and believed to occur mainly via one-electron transfer except for pure Pd/C and Ir/C for which one total electron transfer was estimated. Moreover according to the results hydrogen oxidation reaction is 1-3 magnitudes faster than the oxygen reduction reaction over the as-investigated materials. It seem that both HOR & ORR electrocatalytic activity of the as prepared electrode materials could be attributed to the extent of d-band vacancy and the Pd_xIr_y interatomic distance. According to the results the highest HOR and ORR electrocatalytic activity enhancement is exhibited by PdIr. The order of electrocatalytic activity over the as prepared electrode materials is found to be PdIr>$PdIr_3$>Pd_3Ir>Pd>Ir for HOR and PdIr> Pd_3Ir > $PdIr_3$>Pd>Ir for the ORR.

REFERENCES

1. Tzorbatzoglou, F., *Design and development of a fuel cell system (PEM type)-water electrolysis type PEM: preparation and characterization of low cost electrocatalysts*. 2015, Πανεπιστήμιο Θεσσαλίας. Σχολή Πολυτεχνική. Τμήμα Μηχανολόγων Μηχανικών.
2. Amponsah, N.Y., Troldborg, M., Kington, B., Aalders, I., and Hough, R.L., *Greenhouse gas emissions from renewable energy sources: A review of lifecycle considerations.* Renewable and Sustainable Energy Reviews, 2014. **39**: p. 461-475.
3. Irshad, M., Siraj, K., Raza, R., Ali, A., Tiwari, P., Zhu, B., Rafique, A., Ali, A., Kaleem Ullah, M., and Usman, A., *A Brief Description of High Temperature Solid Oxide Fuel Cell's Operation, Materials, Design, Fabrication Technologies and Performance.* Applied Sciences, 2016. **6**(3): p. 75.
4. Barros, C.P., *Efficiency analysis of hydroelectric generating plants: a case study for Portugal.* Energy Economics, 2008. **30**(1): p. 59-75.
5. Menz, F.C., *Green electricity policies in the United States: case study.* Energy Policy, 2005. **33**(18): p. 2398-2410.
6. Cowie, A.L. and Gardner, W.D., *Competition for the biomass resource: Greenhouse impacts and implications for renewable energy incentive schemes.* Biomass and Bioenergy, 2007. **31**(9): p. 601-607.
7. Prakash, R. and Bhat, I.K., *Energy, economics and environmental impacts of renewable energy systems.* Renewable and Sustainable Energy Reviews, 2009. **13**(9): p. 2716-2721.
8. Gallup, D.L., *Production engineering in geothermal technology: a review.* Geothermics, 2009. **38**(3): p. 326-334.
9. Demirbas, A., *Biofuels securing the planet's future energy needs.* Energy Conversion and Management, 2009. **50**(9): p. 2239-2249.
10. Murugesan, A., Umarani, C., Subramanian, R., and Nedunchezhian, N., *Bio-diesel as an alternative fuel for diesel engines—a review.* Renewable and Sustainable Energy Reviews, 2009. **13**(3): p. 653-662.

11. Subramaniam, D., Murugesan, A., Avinash, A., and Kumaravel, A., *Bio-diesel production and its engine characteristics—An expatiate view.* Renewable and Sustainable Energy Reviews, 2013. **22**: p. 361-370.
12. Balat, M. and Balat, H., *Progress in biodiesel processing.* Applied energy, 2010. **87**(6): p. 1815-1835.
13. Balat, M. and Balat, H., *Recent trends in global production and utilization of bio-ethanol fuel.* Applied energy, 2009. **86**(11): p. 2273-2282.
14. Vogt, K.A., Vogt, D.J., Patel-Weynand, T., Upadhye, R., Edlund, D., Edmonds, R.L., Gordon, J.C., Suntana, A.S., Sigurdardottir, R., and Miller, M., *Bio-methanol: How energy choices in the western United States can help mitigate global climate change.* Renewable Energy, 2009. **34**(1): p. 233-241.
15. Ball, M. and Wietschel, M., *The future of hydrogen–opportunities and challenges.* International Journal of Hydrogen Energy, 2009. **34**(2): p. 615-627.
16. Ehteshami, S.M.M. and Chan, S., *The role of hydrogen and fuel cells to store renewable energy in the future energy network–potentials and challenges.* Energy Policy, 2014. **73**: p. 103-109.
17. Edwards, P.P., Kuznetsov, V.L., David, W.I., and Brandon, N.P., *Hydrogen and fuel cells: towards a sustainable energy future.* Energy Policy, 2008. **36**(12): p. 4356-4362.
18. Ebbing, D. and Gammon, S.D., *General chemistry*. 2010: Cengage Learning.
19. Matthew Bui, W.C.C. *Electrochemistry Basics*. 2016; Available from: https://chem.libretexts.org/Core/Analytical_Chemistry/Electrochemistry/Basics_of_Electrochemistry.
20. Bui, M. *Electrochemical cells*. 2017; Available from: https://chem.libretexts.org/Core/Analytical_Chemistry/Electrochemistry/Basics_of_Electrochemistry/Electrochemical_Cells.
21. Whittaker, E., *A History of the Theories of Aether and Electricity: Vol. I: The Classical Theories; Vol. II: The Modern Theories, 1900-1926*. Vol. 1. 1951: Courier Dover Publications.
22. McIntyre, J.M. and Pham, H.Q., *Electrochemical impedance spectroscopy; a tool for organic coatings optimizations.* Progress in Organic coatings, 1996. **27**(1-4): p. 201-207.

23. Amirudin, A. and Thieny, D., *Application of electrochemical impedance spectroscopy to study the degradation of polymer-coated metals.* Progress in Organic coatings, 1995. **26**(1): p. 1-28.
24. Badwal, S.P., Giddey, S.S., Munnings, C., Bhatt, A.I., and Hollenkamp, A.F., *Emerging electrochemical energy conversion and storage technologies.* Frontiers in chemistry, 2014. **2**.
25. Hollaender, J., *Rapid assessment of food/package interactions by electrochemical impedance spectroscopy (EIS).* Food Additives & Contaminants, 1997. **14**(6-7): p. 617-626.
26. Mabrook, M. and Petty, M., *Effect of composition on the electrical conductance of milk.* Journal of Food Engineering, 2003. **60**(3): p. 321-325.
27. Vielstich, W., Yokokawa, H., and Gasteiger, H.A., *Handbook of fuel cells: fundamentals technology and applications*. 2009: John Wiley & Sons.
28. Larminie, J., Dicks, A., and McDonald, M.S., *Fuel cell systems explained*. Vol. 2. 2003: J. Wiley Chichester, UK.
29. Jonathan, B. *Fuel Cells*. 2013; Available from: https://wiki.uiowa.edu/display/greenergy/Fuel+Cells.
30. Handbook, F.C., *EG&G technical services*. Inc., Albuquerque, NM, DOE/NETL-2004/1206, 2004.
31. Zhao, T., Kreuer, K.-D., and Van Nguyen, T., *Advances in fuel cells*. Vol. 1. 2007: Elsevier.
32. Zhang, J., *PEM fuel cell electrocatalysts and catalyst layers: fundamentals and applications*. 2008: Springer Science & Business Media.
33. climatetechwiki. *Types of Fuel Cells*. 2012; Available from: http://www.climatetechwiki.org/.
34. Mench, M., *Fuel Cell Engines, John Wiley& Sons.* Inc, ISNB, 2008: p. 978-0.
35. Barbir, F., *PEM fuel cells: theory and practice*. 2012: Academic Press.
36. Gontard, L.C., Chang, L.Y., Hetherington, C.J., Kirkland, A.I., Ozkaya, D., and Dunin-Borkowski, R.E., *Aberration-Corrected Imaging of Active Sites on Industrial Catalyst Nanoparticles.* Angewandte Chemie, 2007. **119**(20): p. 3757-3759.
37. Gontard, L.C., DUNIN-BORKOWSKI, R.E., and Ozkaya, D., *Three-dimensional shapes and spatial distributions of Pt and PtCr catalyst*

nanoparticles on carbon black. Journal of microscopy, 2008. **232**(2): p. 248-259.

38. Debe, M.K., *Electrocatalyst approaches and challenges for automotive fuel cells.* Nature, 2012. **486**(7401): p. 43.
39. *Mineral Commodity Summaries.* 2010.
40. *The US Department of Energy (DOE). Energy Efficiency and Renewable Energy.* 2015.
41. Paulus, U., Wokaun, A., Scherer, G., Schmidt, T., Stamenkovic, V., Markovic, N.M., and Ross, P., *Oxygen reduction on high surface area Pt-based alloy catalysts in comparison to well defined smooth bulk alloy electrodes.* Electrochimica Acta, 2002. **47**(22): p. 3787-3798.
42. Koh, S. and Strasser, P., *Electrocatalysis on bimetallic surfaces: modifying catalytic reactivity for oxygen reduction by voltammetric surface dealloying.* Journal of the American Chemical Society, 2007. **129**(42): p. 12624-12625.
43. Stamenkovic, V.R., Fowler, B., Mun, B.S., Wang, G., Ross, P.N., Lucas, C.A., and Marković, N.M., *Improved oxygen reduction activity on Pt3Ni (111) via increased surface site availability.* science, 2007. **315**(5811): p. 493-497.
44. Cui, C., Gan, L., Heggen, M., Rudi, S., and Strasser, P., *Compositional segregation in shaped Pt alloy nanoparticles and their structural behaviour during electrocatalysis.* Nature materials, 2013. **12**(8): p. 765.
45. Zhang, J., Vukmirovic, M.B., Sasaki, K., Nilekar, A.U., Mavrikakis, M., and Adzic, R.R., *Mixed-metal Pt monolayer electrocatalysts for enhanced oxygen reduction kinetics.* Journal of the American Chemical Society, 2005. **127**(36): p. 12480-12481.
46. Zhang, J., Lima, F., Shao, M., Sasaki, K., Wang, J., Hanson, J., and Adzic, R., *Platinum monolayer on nonnoble metal− noble metal core− shell nanoparticle electrocatalysts for O2 reduction.* The Journal of Physical Chemistry B, 2005. **109**(48): p. 22701-22704.
47. Sasaki, K., Naohara, H., Cai, Y., Choi, Y.M., Liu, P., Vukmirovic, M.B., Wang, J.X., and Adzic, R.R., *Core-Protected Platinum Monolayer Shell High-Stability Electrocatalysts for Fuel-Cell Cathodes.* Angewandte Chemie International Edition, 2010. **49**(46): p. 8602-8607.

48. Gong, K., Su, D., and Adzic, R.R., *Platinum-monolayer shell on AuNi0. 5Fe nanoparticle core electrocatalyst with high activity and stability for the oxygen reduction reaction.* Journal of the American Chemical Society, 2010. **132**(41): p. 14364-14366.
49. Sasaki, K., Wang, J., Naohara, H., Marinkovic, N., More, K., Inada, H., and Adzic, R., *Recent advances in platinum monolayer electrocatalysts for oxygen reduction reaction: Scale-up synthesis, structure and activity of Pt shells on Pd cores.* Electrochimica Acta, 2010. **55**(8): p. 2645-2652.
50. Wang, D., Xin, H.L., Hovden, R., Wang, H., Yu, Y., Muller, D.A., DiSalvo, F.J., and Abruña, H.D., *Structurally ordered intermetallic platinum-cobalt core-shell nanoparticles with enhanced activity and stability as oxygen reduction electrocatalysts.* Nature materials, 2013. **12**(1): p. 81.
51. Xin, H.L., Mundy, J.A., Liu, Z., Cabezas, R., Hovden, R., Kourkoutis, L.F., Zhang, J., Subramanian, N.P., Makharia, R., and Wagner, F.T., *Atomic-resolution spectroscopic imaging of ensembles of nanocatalyst particles across the life of a fuel cell.* Nano letters, 2011. **12**(1): p. 490-497.
52. Borup, R., Meyers, J., Pivovar, B., Kim, Y.S., Mukundan, R., Garland, N., Myers, D., Wilson, M., Garzon, F., and Wood, D., *Scientific aspects of polymer electrolyte fuel cell durability and degradation.* Chemical reviews, 2007. **107**(10): p. 3904-3951.
53. Gasteiger, H.A., Kocha, S.S., Sompalli, B., and Wagner, F.T., *Activity benchmarks and requirements for Pt, Pt-alloy, and non-Pt oxygen reduction catalysts for PEMFCs.* Applied Catalysis B: Environmental, 2005. **56**(1): p. 9-35.
54. Wagner, F.T., Lakshmanan, B., and Mathias, M.F., *Electrochemistry and the future of the automobile.* J. Phys. Chem. Lett, 2010. **1**(14): p. 2204-2219.
55. Proietti, E., Jaouen, F., Lefèvre, M., Larouche, N., Tian, J., Herranz, J., and Dodelet, J.-P., *Iron-based cathode catalyst with enhanced power density in polymer electrolyte membrane fuel cells.* Nature communications, 2011. **2**: p. 416.
56. *U.S. Department of Energy (Hydrogen and Fuel Cells Program).* 2016.
57. *U.S. Department of Energy (Hydrogen and Fuel Cells Program).* 2013.

58. James, B.D., Huya-Kouadio, J.M., Houchins, C., and DeSantis, D.A., *Mass Production Cost Estimation of Direct H2 PEM Fuel Cell Systems for Transportation Applications (2012-2016)*. 2016, Strategic Analysis Inc., Arlington, VA (United States).
59. Deng, X., Wang, H., Huang, H., and Ouyang, M., *Hydrogen flow chart in China.* International Journal of Hydrogen Energy, 2010. **35**(13): p. 6475-6481.
60. Kreith, F. and West, R., *Fallacies of a hydrogen economy: a critical analysis of hydrogen production and utilization.* Transactions of the ASME-M-Journal of Energy Resources Technology, 2004. **126**(4): p. 249-257.
61. Brouzgou, A., Song, S., and Tsiakaras, P., *Low and non-platinum electrocatalysts for PEMFCs: current status, challenges and prospects.* Applied Catalysis B: Environmental, 2012. **127**: p. 371-388.
62. Shu, J., Grandjean, B., Neste, A.V., and Kaliaguine, S., *Catalytic palladium-based membrane reactors: A review.* The Canadian Journal of Chemical Engineering, 1991. **69**(5): p. 1036-1060.
63. Yun, S. and Oyama, S.T., *Correlations in palladium membranes for hydrogen separation: a review.* Journal of membrane science, 2011. **375**(1): p. 28-45.
64. Hatlevik, Ø., Gade, S.K., Keeling, M.K., Thoen, P.M., Davidson, A., and Way, J.D., *Palladium and palladium alloy membranes for hydrogen separation and production: history, fabrication strategies, and current performance.* Separation and Purification Technology, 2010. **73**(1): p. 59-64.
65. Lou, X.W.D., Archer, L.A., and Yang, Z., *Hollow micro-/nanostructures: Synthesis and applications.* Advanced Materials, 2008. **20**(21): p. 3987-4019.
66. Liang, H.P., Zhang, H.M., Hu, J.S., Guo, Y.G., Wan, L.J., and Bai, C.L., *Pt hollow nanospheres: facile synthesis and enhanced electrocatalysts.* Angewandte Chemie, 2004. **116**(12): p. 1566-1569.
67. Łukaszewski, M., Grdeń, M., and Czerwiński, A., *Hydrogen insertion into Pd–Pt–Rh alloy limited volume electrodes (LVEs)☆☆ Keynote Lecture.* Journal of Physics and Chemistry of Solids, 2004. **65**(2): p. 523-528.
68. ur Rehman, A., Hossain, S.S., ur Rahman, S., Ahmed, S., and Hossain, M.M., *WO 3 modification effects on Pt–Pd/WO 3-OMC electrocatalysts for formic acid oxidation.* Applied Catalysis A: General, 2014. **482**: p. 309-317.

69. Gade, S.K., Keeling, M.K., Davidson, A.P., Hatlevik, O., and Way, J.D., *Palladium–ruthenium membranes for hydrogen separation fabricated by electroless co-deposition.* International Journal of Hydrogen Energy, 2009. **34**(15): p. 6484-6491.

70. Ham, D.J., Pak, C., Bae, G.H., Han, S., Kwon, K., Jin, S.-A., Chang, H., Choi, S.H., and Lee, J.S., *Palladium–nickel alloys loaded on tungsten carbide as platinum-free anode electrocatalysts for polymer electrolyte membrane fuel cells.* Chemical Communications, 2011. **47**(20): p. 5792-5794.

71. Łukaszewski, M., Grdeń, M., and Czerwiński, A., *Hydrogen electrosorption in Pd–Pt–Rh alloys.* Journal of Electroanalytical Chemistry, 2004. **573**(1): p. 87-98.

72. Kwon, K., Jin, S.-a., Lee, K.H., You, D.J., and Pak, C., *Performance enhancement of Pd-based hydrogen oxidation catalysts using tungsten oxide.* Catalysis Today, 2014. **232**: p. 175-178.

73. Lee, H., Habas, S.E., Somorjai, G.A., and Yang, P., *Localized Pd overgrowth on cubic Pt nanocrystals for enhanced electrocatalytic oxidation of formic acid.* Journal of the American Chemical Society, 2008. **130**(16): p. 5406-5407.

74. Salvador-Pascual, J., Citalán-Cigarroa, S., and Solorza-Feria, O., *Kinetics of oxygen reduction reaction on nanosized Pd electrocatalyst in acid media.* Journal of Power Sources, 2007. **172**(1): p. 229-234.

75. Shao, M., *Palladium-based electrocatalysts for hydrogen oxidation and oxygen reduction reactions.* Journal of Power Sources, 2011. **196**(5): p. 2433-2444.

76. Shao, M., Liu, P., Zhang, J., and Adzic, R., *Origin of enhanced activity in palladium alloy electrocatalysts for oxygen reduction reaction.* The Journal of Physical Chemistry B, 2007. **111**(24): p. 6772-6775.

77. Ramos-Sánchez, G., Yee-Madeira, H., and Solorza-Feria, O., *PdNi electrocatalyst for oxygen reduction in acid media.* International Journal of Hydrogen Energy, 2008. **33**(13): p. 3596-3600.

78. Antolini, E., Zignani, S.C., Santos, S.F., and Gonzalez, E.R., *Palladium-based electrodes: A way to reduce platinum content in polymer electrolyte membrane fuel cells.* Electrochimica Acta, 2011. **56**(5): p. 2299-2305.

79. Wang, W., Zheng, D., Du, C., Zou, Z., Zhang, X., Xia, B., Yang, H., and Akins, D.L., *Carbon-supported Pd-Co bimetallic nanoparticles as electrocatalysts for the oxygen reduction reaction.* Journal of Power Sources, 2007. **167**(2): p. 243-249.

80. Martínez-Casillas, D., Vázquez-Huerta, G., Pérez-Robles, J., and Solorza-Feria, O., *Electrocatalytic reduction of dioxygen on PdCu for polymer electrolyte membrane fuel cells*. Journal of Power Sources, 2011. **196**(10): p. 4468-4474.

81. Wang, X., Kariuki, N., Vaughey, J.T., Goodpaster, J., Kumar, R., and Myers, D.J., *Bimetallic Pd–Cu oxygen reduction electrocatalysts.* Journal of The Electrochemical Society, 2008. **155**(6): p. B602-B609.

82. Xu, C., Zhang, Y., Wang, L., Xu, L., Bian, X., Ma, H., and Ding, Y., *Nanotubular mesoporous PdCu bimetallic electrocatalysts toward oxygen reduction reaction.* Chemistry of materials, 2009. **21**(14): p. 3110-3116.

83. Kariuki, N.N., Wang, X., Mawdsley, J.R., Ferrandon, M.S., Niyogi, S.G., Vaughey, J.T., and Myers, D.J., *Colloidal synthesis and characterization of carbon-supported Pd− Cu nanoparticle oxygen reduction electrocatalysts.* Chemistry of materials, 2010. **22**(14): p. 4144-4152.

84. Shao, M.-H., Sasaki, K., and Adzic, R.R., *Pd− Fe nanoparticles as electrocatalysts for oxygen reduction.* Journal of the American Chemical Society, 2006. **128**(11): p. 3526-3527.

85. Tarasevich, M., Zhutaeva, G., Bogdanovskaya, V., Radina, M., Ehrenburg, M., and Chalykh, A., *Oxygen kinetics and mechanism at electrocatalysts on the base of palladium–iron system.* Electrochimica Acta, 2007. **52**(15): p. 5108-5118.

86. Holton, O.T. and Stevenson, J.W., *The role of platinum in proton exchange membrane fuel cells.* Platinum Metals Review, 2013. **57**(4): p. 259-271.

87. Ioroi, T. and Yasuda, K., *Platinum-iridium alloys as oxygen reduction electrocatalysts for polymer electrolyte fuel cells.* Journal of The Electrochemical Society, 2005. **152**(10): p. A1917-A1924.

88. Wang, C.-H., Hsu, H.-C., and Wang, K.-C., *Iridium-decorated Palladium–Platinum core–shell catalysts for oxygen reduction reaction in proton*

exchange membrane fuel cell. Journal of colloid and interface science, 2014. **427**: p. 91-97.

89. Ioroi, T., Kitazawa, N., Yasuda, K., Yamamoto, Y., and Takenaka, H., *Iridium oxide/platinum electrocatalysts for unitized regenerative polymer electrolyte fuel cells.* Journal of The Electrochemical Society, 2000. **147**(6): p. 2018-2022.
90. Härk, E., Jäger, R., Kasatkin, P., Tallo, I., Möller, P., Romann, T., Kanarbik, R., Joost, U., Aruväli, J., and Lust, E., *The platinum-group metal based catalysts for oxygen electroreduction reaction.*
91. Todoroki, N., Watanabe, H., Kondo, T., Kaneko, S., and Wadayama, T., *Highly Enhanced Oxygen Reduction Reaction Activity and Electrochemical Stability of Pt/Ir (111) Bimetallic Surfaces.* Electrochimica Acta, 2016. **222**: p. 1616-1621.
92. Song, S., Wang, Y., and Shen, P.K., *Pulse-microwave assisted polyol synthesis of highly dispersed high loading Pt/C electrocatalyst for oxygen reduction reaction.* Journal of Power Sources, 2007. **170**(1): p. 46-49.
93. Song, S., Liu, J., Shi, J., Liu, H., Maragou, V., Wang, Y., and Tsiakaras, P., *The effect of microwave operation parameters on the electrochemical performance of Pt/C catalysts.* Applied Catalysis B: Environmental, 2011. **103**(3): p. 287-293.
94. Wang, X., Tang, Y., Gao, Y., and Lu, T., *Carbon-supported Pd–Ir catalyst as anodic catalyst in direct formic acid fuel cell.* Journal of Power Sources, 2008. **175**(2): p. 784-788.
95. Radmilovic, V., Gasteiger, H., and Ross, P., *Structure and chemical composition of a supported Pt-Ru electrocatalyst for methanol oxidation.* Journal of Catalysis, 1995. **154**(1): p. 98-106.
96. Irhayem, E.A., Elzanowska, H., Jhas, A.S., Skrzynecka, B., and Birss, V., *Glucose detection based on electrochemically formed Ir oxide films.* Journal of Electroanalytical Chemistry, 2002. **538**: p. 153-164.
97. Hsieh, C.-T., Liu, Y.-Y., Cheng, Y.-S., and Chen, W.-Y., *Microwave-assisted synthesis and pulse electrodeposition of palladium nanocatalysts on carbon nanotube-based electrodes.* Electrochimica Acta, 2011. **56**(18): p. 6336-6344.

98. Quaino, P., Fernandez, J., de Chialvo, M.G., and Chialvo, A., *Hydrogen oxidation reaction on microelectrodes: Analysis of the contribution of the kinetic routes.* Journal of Molecular Catalysis A: Chemical, 2006. **252**(1): p. 156-162.

99. Gabrielli, C., Grand, P., Lasia, A., and Perrot, H., *Investigation of hydrogen adsorption and absorption in palladium thin films II. Cyclic voltammetry.* Journal of The Electrochemical Society, 2004. **151**(11): p. A1937-A1942.

100. Conway, B. and Tilak, B., *Interfacial processes involving electrocatalytic evolution and oxidation of H 2, and the role of chemisorbed H.* Electrochimica Acta, 2002. **47**(22): p. 3571-3594.

101. Escudero-Cid, R., Varela, A., Hernández-Fernández, P., Fatás, E., and Ocón, P., *The effect of functionalised multi-walled carbon nanotubes in the hydrogen electrooxidation reaction in reactive currents impurified with CO.* International Journal of Hydrogen Energy, 2014. **39**(10): p. 5063-5073.

102. Chen, D., Cui, P., He, H., Liu, H., and Yang, J., *Highly catalytic hollow palladium nanoparticles derived from silver@ silver–palladium core–shell nanostructures for the oxidation of formic acid.* Journal of Power Sources, 2014. **272**: p. 152-159.

103. Durst, J., Siebel, A., Simon, C., Hasche, F., Herranz, J., and Gasteiger, H., *New insights into the electrochemical hydrogen oxidation and evolution reaction mechanism.* Energy & Environmental Science, 2014. **7**(7): p. 2255-2260.

104. Chen, D., Cui, P., He, H., Liu, H., and Yang, J., *Highly catalytic hollow palladium nanoparticles derived from silver@silver–palladium core–shell nanostructures for the oxidation of formic acid.* Journal of Power Sources, 2014. **272**(0): p. 152-159.

105. Durst, J., Siebel, A., Simon, C., Hasche, F., Herranz, J., and Gasteiger, H.A., *New insights into the electrochemical hydrogen oxidation and evolution reaction mechanism.* Energy & Environmental Science, 2014. **7**(7): p. 2255-2260.

106. Langhus, D.L., *Modern Electrochemistry, Volume 1: Ionics (Bockris, John O'M.; Reddy, Amulya KN)*. 1999, ACS Publications.

107. Mello, R.M. and Ticianelli, E.A., *Kinetic study of the hydrogen oxidation reaction on platinum and Nafion® covered platinum electrodes.* Electrochimica Acta, 1997. **42**(6): p. 1031-1039.

108. Gottesfeld, S., *Fuel cell science: theory, fundamentals, and biocatalysis*. Vol. 9. 2011: John Wiley & Sons.

109. Bron, M., Fiechter, S., Hilgendorff, M., and Bogdanoff, P., *Catalysts for oxygen reduction from heat-treated carbon-supported iron phenantroline complexes.* Journal of applied electrochemistry, 2002. **32**(2): p. 211-216.

110. Sánchez-Sánchez, C.M. and Bard, A.J., *Hydrogen peroxide production in the oxygen reduction reaction at different electrocatalysts as quantified by scanning electrochemical microscopy.* Analytical chemistry, 2009. **81**(19): p. 8094-8100.

111. Han, S.J., Jung, H.J., Shim, J.H., Kim, H.-C., Sung, S.-J., Yoo, B., Lee, D.H., Lee, C., and Lee, Y., *Non-platinum oxygen reduction electrocatalysts based on carbon-supported metal–polythiophene composites.* Journal of Electroanalytical Chemistry, 2011. **655**(1): p. 39-44.

112. Knani, S., Chirchi, L., Napporn, W., Baranton, S., Léger, J., and Ghorbel, A., *Promising ternary Pt–Co–Sn catalyst for the oxygen reduction reaction.* Journal of Electroanalytical Chemistry, 2015. **738**: p. 145-153.

113. Macia, M., Campina, J., Herrero, E., and Feliu, J., *On the kinetics of oxygen reduction on platinum stepped surfaces in acidic media.* Journal of Electroanalytical Chemistry, 2004. **564**: p. 141-150.

114. Pickup, P.G. and Birss, V.I., *The kinetics of charging and discharging of iridium oxide films in aqueous and non-aqueous media.* Journal of electroanalytical chemistry and interfacial electrochemistry, 1988. **240**(1-2): p. 185-199.